Lattice distortion and magnetism of $3d$-t_{2g} perovskite oxides

I. V. Solovyev*
Computational Materials Science Center, National Institute for Materials Science, 1-2-1 Sengen, Tsukuba, Ibaraki 305-0047, Japan
(Received 1 February 2006; revised manuscript received 15 May 2006; published 9 August 2006)

Several puzzling aspects of interplay of the experimental lattice distortion and the magnetic behavior of four narrow t_{2g}-band perovskite oxides ($YTiO_3$, $LaTiO_3$, YVO_3, and $LaVO_3$) are clarified using results of first-principles electronic structure calculations. First, we derive parameters of the effective Hubbard-type Hamiltonian for the isolated t_{2g} bands using newly developed downfolding method for the kinetic-energy part and a hybrid approach, based on the combination of the random-phase approximation and the constraint local-density approximation, for the screened Coulomb interaction part. Apart from the above-mentioned approximation, the procedure of constructing the model Hamiltonian is totally parameter free. The results are discussed in terms of the Wannier functions localized around transition-metal sites. The obtained Hamiltonian was solved using a number of techniques, including the mean-field Hartree-Fock (HF) approximation, the second-order perturbation theory for the correlation energy, and a variational superexchange theory, which takes into account the multiplet structure of the atomic states. We argue that the crystal distortion has a profound effect not only on the values of the crystal-field (CF) splitting, but also on the behavior of transfer integrals and even the screened Coulomb interactions. Even though the CF splitting is not particularly large to fully quench the orbital degrees of freedom (ODF), the crystal distortion imposes a severe constraint on the form of the possible orbital states, which favor the formation of the experimentally observed magnetic structures in $YTiO_3$, YVO_3, and $LaVO_3$ even at the level of mean-field HF approximation. Particularly, $LaVO_3$ presents an interesting example of the system where the ODF are well quenched only in one of the monoclinic planes and remain relatively flexible in the second plane, leaving some room for the orbital fluctuations. It is also remarkable that for all three compounds, the main results of all-electron calculations can be successfully reproduced in our minimal model derived for the isolated t_{2g} bands. We confirm that such an agreement is possible only when the nonsphericity of the Madelung potential is explicitly included into the model. Beyond the HF approximation, the correlation effects systematically improve the agreement with the experimental data and additionally stabilize the experimentally observed G- and C-type antiferromagnetic states in YVO_3 and $LaVO_3$. Using the same type of approximations we could not obtain the correct magnetic ground state for $LaTiO_3$. However, we expect that the situation may change by systematically improving the level of approximations for treating the correlation effects.

DOI: 10.1103/PhysRevB.74.054412 PACS number(s): 71.28.+d, 75.25.+z, 71.15.−m, 71.10.−w

I. INTRODUCTION

The transition-metal perovskite oxides ABO_3 (with A=Y, La, or other trivalent rare-earth ion, and B=Ti or V) are regarded as some of the key materials for understanding the strong coupling among spin, orbital, and lattice degrees of freedom in correlated electron systems.[1]

According to the electronic structure calculations in the local-density approximation (LDA), all these compounds can be classified as the "t_{2g} systems," as all of them have a common transition-metal t_{2g} band, located near the Fermi level, which is sandwiched between oxygen $2p$ band and a hybrid transition-metal e_g band, which overlaps with either Y($4d$) or La($5d$) bands (see Fig. 1). The number of electrons donated by each Ti and V atom into the t_{2g} band is correspondingly one and two. These electrons are subjected to the strong Coulomb repulsion. The physics of Coulomb correlations is greatly oversimplified by LDA and requires some considerable improvement of this approximation, which currently processes in the direction of merging LDA with various model approaches for strongly correlated systems.[2–5] Nevertheless, even for strongly correlated systems, LDA continues to play an important role as it allows us to combine the physics of Coulomb correlations with the lattice distortions, and treat the second part of the problem in a fully *ab initio* fashion, without any adjustable parameters.

Although the origin of the lattice distortion in the t_{2g} perovskite oxides is not fully understood, it is definitely strong and exhibits an appreciable material dependence, which can be seen even visually in Fig. 2. The interplay of this lattice distortion with the Coulomb correlations seems to be the key factor for understanding of the large variation of the magnetic properties among these perovskite oxides. The difference exists not only between titanites and vanadates, but also within each group of formally isoelectronic materials, depending on whether they are built of Y or La. The latter example seems to be a clear experimental manifestation of the distortion effect, arising from the different size of trivalent ions (smaller Y^{3+} versus larger La^{3+}). All these differences are reflected in the famous phase diagram of the distorted t_{2g} perovskite oxides, where each compound has a distinct magnetic structure: $YTiO_3$ is a ferromagnet;[6–10] $LaTiO_3$ is a three-dimensional (G-type) antiferromagnet;[11,12] at the low temperature, YVO_3 forms the G-type antiferromagnetic (AFM) structure, which transforms to a chainlike (C-type) antiferromagnetic structure at around 77 K;[13–16] while $LaVO_3$ is the C-type antiferromagnet in the whole temperature range below the magnetic transition temperature.[17,18]

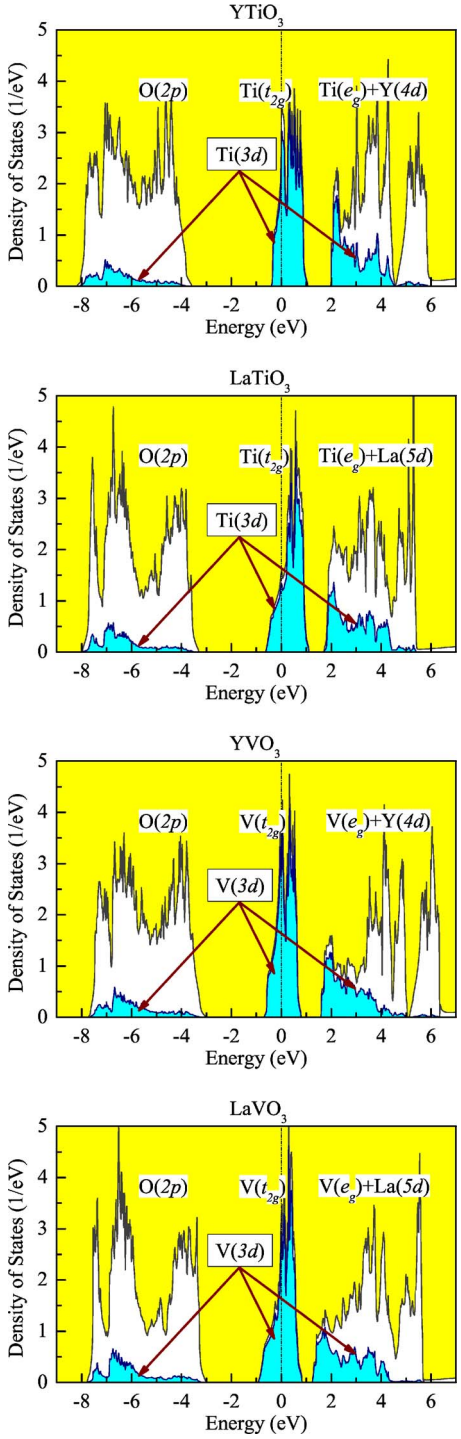

FIG. 1. (Color online) Total and partial densities of states for $YTiO_3$, $LaTiO_3$, YVO_3 (orthorhombic phase), and $LaVO_3$ in the local-density approximation. The shaded area shows the contributions of the transition-metal 3*d* states. Other symbols show the positions of the main bands. The Fermi level is at zero energy.

On the theoretical side, the magnetic phase diagram of t_{2g} perovskite oxides has been intensively studied using both models (Refs. 19–24) and first-principles electronic structure calculations (Refs. 25–33). The problem is still far from being understood, and remains to be the subject of numerous contradictions and debates. Surprisingly that at the present stage there is no clear consensus not only between model and first-principles electronic structure communities, but even between researchers working in each of these fields. Presumably, the most striking example is $LaTiO_3$, where in order to explain the experimentally observed *G*-type AFM ground state, two different models, which practically exclude each other, have been proposed. One is the model of orbital liquid, which implies that the crystal distortion is small and the *(quasi-) degeneracy of the atomic* t_{2g} *levels is preserved in the real crystalline environment*.[20] Another model is based on the theory of the crystal-field (CF) splitting, *which lifts this orbital degeneracy* and stabilizes one particular type the orbital ordering compatible with the *G*-type AFM phase.[23,24] The situation in the area of first-principles electronic structure calculations is controversial as well. Although majority of researchers working in this field now agree that, in order to describe properly the electronic structure of t_{2g} perovskite oxides, it is necessary go beyond the conventional LDA and incorporate the effects of intraatomic Coulomb correlations, this merging is typically done in a semiempirical way, as it relies on a certain number of adjustable parameters, postulates, and the form of the basis functions used for the implementation of additional corrections on the top of LDA.[2–4] There are also certain differences regarding both definitions and approximations used for the CF splitting in the electronic structure calculations, which will be discussed in Sec. III A. Since the magnetic properties of t_{2g} perovskite oxides are extremely sensitive to all these details, it is not surprising that there is a substantial variation in the results of first-principles calculations, which sometimes yield even qualitatively different conclusions about the direction of the CF splitting as well as the form of the magnetic ground state.[28,31–33] The problem is not only in the numerical accuracy of calculations. Simply, the error-bar caused by the additional assumptions about the form and magnitude of intraatomic Coulomb interactions, which are largely empirical, already exceeds those small differences of physical quantities, which we typically deal with in the case of t_{2g} perovskite oxides. In the light of these controversies, it seems that the formulation of the method, which would be free of any adjustable parameters, becomes a real cornerstone of electronic structure calculations for strongly correlated systems.

Therefore, the main motivation of the present work is twofold.

(i) In our previous work (Ref. 34) we have proposed a method of construction of the effective Hubbard-type model for the states located near the Fermi level on the basis of first-principles electronic structure calculations. In the present work we apply this strategy to the t_{2g} states of the distorted perovskite oxides. Namely, we will derive parameters of the effective multiorbital Hubbard Hamiltonian for the t_{2g} bands and solve this Hamiltonian using a number of techniques, including the Hartree-Fock (HF) approximation, the perturbation theory for the correlation energy, and the theory of superexchange interactions, which takes into account the effects of the multiplet structure of the atomic states. Of course, our method is based on a number of approximation, which have been introduced in Ref. 34 and will be briefly discussed in Sec. III. However, we would like to emphasize from the very beginning that our policy here was

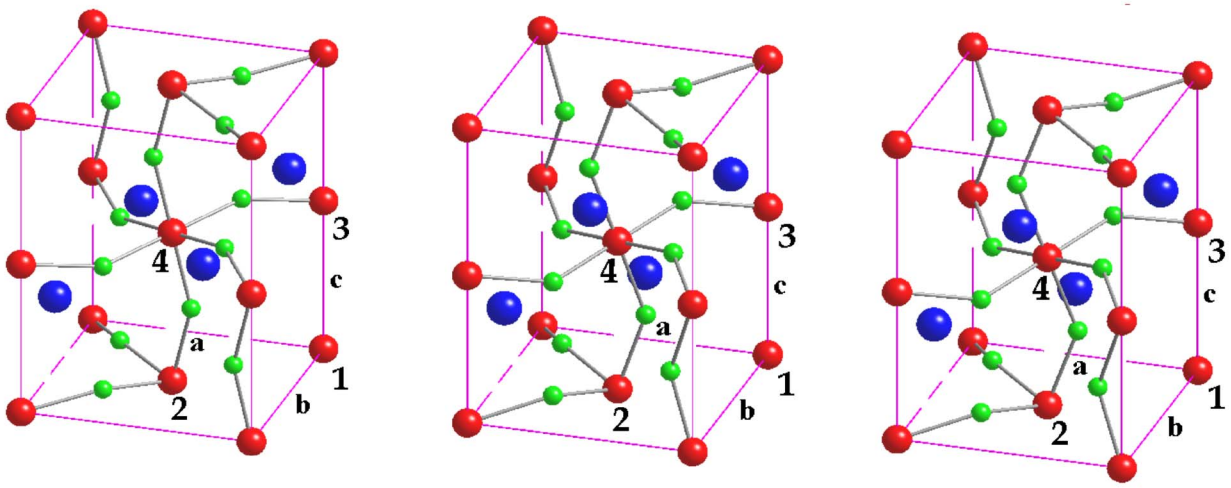

FIG. 2. (Color online) Crystal structure of orthorhombic $LaTiO_3$ (left), $YTiO_3$ (middle), and YVO_3 (right). The La and Y atoms are indicated by the big (blue) dark spheres, the Ti and V atoms are indicated by the medium (red) dark gray spheres, and the oxygen atoms are indicated by the small (green) light gray spheres. The symbols **a**, **b**, and **c** stand for the orthorhombic translations. The symbols 1–4 denote the transition-metal sites, which form the unit cell of the distorted perovskite oxides.

not to use any adjustable parameters apart from the approximations introduced in Ref. 34. Thus, we believe that it poses a severe test for the proposed method, and the obtained results should clearly demonstrate that our general strategy, which can be expressed by the formula: *first-principles electronic structure calculations→construction of the model Hamiltonian→solution of this model Hamiltonian*,[5,34] is indeed very promising. For example, at the HF level, using relatively simple model Hamiltonian, which is limited exclusively by the t_{2g} bands, we will be able to reproduce the main results of all-electron LDA+U calculations.[27,29] Furthermore, due to simplicity of the model Hamiltonian we can easily go beyond the HF approximation and consider the correlation effects.

(ii) Why do we need to convert results of first-principles electronic structure calculations into a model? Apart from a purely technical reason to reduce the size of the physical Hilbert space in order to make it accessible for many-electron calculations,[4,5] the story of distorted t_{2g} perovskite oxides clearly shows that the model consideration has yet another advantage, which sometimes is not sufficiently appreciated by the computational community. It is true that the field of first-principles electronic structure calculations is currently on the rise, and calculations of the basic properties for many materials will soon become a matter of routine. However, the methods of electronic structure calculations are based on some approximations, the limitations of which should be clearly understood. Furthermore, like the experiment data, the results of first-principles electronic structure calculations will always require some interpretation, which would transform the world of numbers and trends into a "parallel world" of rationalized model categories capturing the essential part of these calculations. The understanding of the results of calculations in terms of these categories opens a way, on the one hand, to the material engineering of compounds with a desired set of properties, and, on the other way, to the "engineering" of the new methods of electronic structure calculations in the direction of further elucidation and overcoming the defects of the existing approximations. In this work we will illustrate how the results of first-principles calculations for distorted perovskite oxides can be interpreted in terms of a limited number of model parameters, such as the crystal-field splitting, transfer integrals, and intra-atomic Coulomb interactions, which can be regarded as the basic operating blocks for understanding the properties of these materials as well as the limitations of approximations existing in the methods of electronic structure calculations. Particularly, we will explicitly show that the atomic-spheres approximation (ASA), which was employed in the series of publications (Refs. 28 and 30–32), is not enough as it neglects the nonsphericity of the Madelung potential. The latter plays an important role and in a number of cases predetermines the character of the magnetic ground state of the distorted perovskite oxides. We will also show that once the parameters of Coulomb interactions are determined from the first principles, the commonly used mean-field HF approximation does not necessarily guarantee the right answer for the magnetic properties of t_{2g} perovskite oxides. However, we will argue that this is a normal situation, and in the majority of cases, a better agreement with the experimental data can be obtained by systematically including the correlation effects beyond the HF approximation. In this sense, our strategy is completely different from conventional LDA+U calculations, where the on-site Coulomb interaction U is typically treated as an adjustable parameter (e.g., Refs. 27, 29, and 31–33). By changing U, one can certainly get a better numerical agreement with some experimental data already at the HF level. However, one should clearly understand that such an empirical treatment actually disguises the actual role played by the correlation effects in the narrow-band compounds.

The rest of the paper is organized as follows. In Sec. II we will briefly remind the main details of crystal and magnetic structure of the distorted perovskite oxides. The procedure of

constructing the model Hamiltonian as well as the results of calculations of the CF splitting, transfer integrals, and intraatomic Coulomb interactions for the isolated t_{2g} band will be briefly explained in Sec. III. Particularly, in Sec. III A we will discuss the highly controversial situation around the values of the CF splitting extracted from electronic structure calculations,[28,30–32] and argue that the main differences are caused by two factors: (i) certain arbitrariness with the choice of the Wannier functions for distorted perovskite oxides; (ii) additional approximations used for the nonspherical part of the crystalline potential inside atomic spheres. The methods of solution of the model Hamiltonian will be described in Sec. IV, and the results of these calculations will be presented in Sec. V. Finally, in Sec. VI we will summarize the main results of our work.

II. CRYSTAL AND MAGNETIC STRUCTURES

The distorted perovskite oxides contain four formula units in the primitive cell. The transition-metal atoms are located at $(0,0,0)$ (site 1), $(\mathbf{a}/2,\mathbf{b}/2,0)$ (site 2), $(0,0,\mathbf{c}/2)$ (site 3), and $(\mathbf{a}/2,\mathbf{b}/2,\mathbf{c}/2)$ (site 4), in terms of three primitive translations: **a**, **b**, and **c** (see Fig. 2). The distortion can be either orthorhombic or monoclinic.

The space group of the orthorhombic phase is D_{2h}^{16} (in the Schönflies notations or *Pbnm* in the Hermann-Maguin notations, No. 62 in the International Tables). In this case all transition-metal sites are equivalent and can be transformed to each other using symmetry operations of the D_{2h}^{16} group.

The space group of the monoclinic phase is C_{2h}^{5} ($P2_1/a$, No. 14 in the International Tables).[14,35] In this case, there are two nonequivalent pairs of transition-metal sites: (1,2) and (3,4). Each pair is allocated within one **ab** plane, so that the atoms of this pair can be transformed to each other using symmetry operations of the C_{2h}^{5} group. However, there is no symmetry operation, which connects the different pairs of atoms from neighboring **ab** planes.

All calculations have been performed using experimental lattice parameters and atomic positions. The experimental data have been taken from the following papers: Ref. 6 for $YTiO_3$ (the measurements have been done for the room temperature $T=293$ K), Ref. 12 for $LaTiO_3$ ($T=8$ K), Ref. 14 for YVO_3 ($T=65$ K and 100 K, for the orthorhombic and monoclinic phase, respectively), and Ref. 18 for $LaVO_3$ ($T=10$ K).

There are five possible magnetic structure, which can be obtained by associating with each transition-metal site either positive ($\uparrow$) or negative ($\downarrow$) direction of the spin, without enlarging the unit cell. Therefore, each magnetic structure can be denoted by means of four vectors associated with the transition-metal sites (1, 2, 3, 4). They are

(1) $(\uparrow\uparrow\uparrow\uparrow)$, which is called the ferromagnetic (F) phase;

(2) $(\uparrow\uparrow\downarrow\downarrow)$, the layered ($A$-type) antiferromagnetic phase;

(3) $(\uparrow\downarrow\uparrow\downarrow)$, the chainlike ($C$-type) antiferromagnetic phase;

(4) $(\uparrow\downarrow\downarrow\uparrow)$, the totally antiferromagnetic (G-type) phase;

(5) $(\downarrow\uparrow\uparrow\uparrow)$, the spin-flip phase. In the monoclinic structure, there are two different spin-flip phases: $(\downarrow\uparrow\uparrow\uparrow)$ and $(\uparrow\uparrow\downarrow\uparrow)$, which will be denoted as flip I and flip II, respectively.

Similar classification can be used for the orbital ordering. Typically, two orthogonal orbitals belonging to different transition-metal sites are said to be ordered antiferromagnetically, although such a definition is not unique.[36]

III. MODEL HAMILTONIAN

Our first goal is the construction of the effective multiorbital Hubbard model for the isolated t_{2g} bands,

$$\hat{\mathcal{H}} = \sum_{\mathbf{R}\mathbf{R}'} \sum_{\alpha\beta} h_{\mathbf{R}\mathbf{R}'}^{\alpha\beta} \hat{c}_{\mathbf{R}\alpha}^{\dagger} \hat{c}_{\mathbf{R}'\beta} + \frac{1}{2} \sum_{\mathbf{R}} \sum_{\alpha\beta\gamma\delta} U_{\alpha\beta\gamma\delta} \hat{c}_{\mathbf{R}\alpha}^{\dagger} \hat{c}_{\mathbf{R}\gamma}^{\dagger} \hat{c}_{\mathbf{R}\beta} \hat{c}_{\mathbf{R}\delta}, \tag{1}$$

where $\hat{c}_{\mathbf{R}\alpha}^{\dagger}$ ($\hat{c}_{\mathbf{R}\alpha}$) creates (annihilates) an electron in the Wannier orbital $\tilde{W}_{\mathbf{R}}^{\alpha}$ of the transition-metal site **R**, and α is a joint index, incorporating all remaining (spin and orbital) degrees of freedom. The matrix $\hat{h}_{\mathbf{R}\mathbf{R}'} = \| h_{\mathbf{R}\mathbf{R}'}^{\alpha\beta} \|$ parametrizes the kinetic energy of electrons, where the site-diagonal part ($\mathbf{R}=\mathbf{R}'$) describes the local level-splitting, caused by the crystal-field and (or) the spin-orbit interaction, and the off-diagonal part ($\mathbf{R}\neq\mathbf{R}'$) stands for the transfer integrals.

$$U_{\alpha\beta\gamma\delta} = \int d\mathbf{r} \int d\mathbf{r}' \tilde{W}_{\mathbf{R}}^{\alpha\dagger}(\mathbf{r}) \tilde{W}_{\mathbf{R}}^{\beta}(\mathbf{r}) v_{\mathrm{scr}}(\mathbf{r}-\mathbf{r}') \tilde{W}_{\mathbf{R}}^{\gamma\dagger}(\mathbf{r}') \tilde{W}_{\mathbf{R}}^{\delta}(\mathbf{r}')$$
$$\equiv \langle \tilde{W}_{\mathbf{R}}^{\alpha} \tilde{W}_{\mathbf{R}}^{\gamma} | v_{\mathrm{scr}} | \tilde{W}_{\mathbf{R}}^{\beta} \tilde{W}_{\mathbf{R}}^{\delta} \rangle$$

are the matrix elements of *screened* Coulomb interaction $v_{\mathrm{scr}}(\mathbf{r}-\mathbf{r}')$, which are supposed to be diagonal with respect to the site indices. As we shall see below, $U_{\alpha\beta\gamma\delta}$ can also depend on the site index **R**. Even in the orthorhombic structure, the Coulomb matrix elements at different transition-metal sites are related by some unitary transformations. In the monoclinic structure, there are two different sets of parameters of Coulomb interactions associated with different **ab** planes. However, for the sake of simplicity, here and throughout in this paper we drop the index **R** in the notation of the Coulomb matrix elements.

The parameters of the Hubbard Hamiltonian (1) can be derived from the first principles, starting from the electronic structure in LDA. This procedure has been already discussed in details in Ref. 34. Here we only remind the main ideas and present the results for the distorted perovskite oxides.

All calculations have been performed using the linear muffin-tin-orbital (LMTO) method in the atomic-spheres approximation.[37] We have also considered the additional corrections to the crystal-field splitting, coming from the nonsphericity of electron-ion interactions, beyond conventional ASA.[34]

A. Kinetic-energy part, controversy about the crystal-field splitting

The kinetic-energy part of the Hubbard Hamiltonian was constructed using the downfolding method.[28,34] It yields a

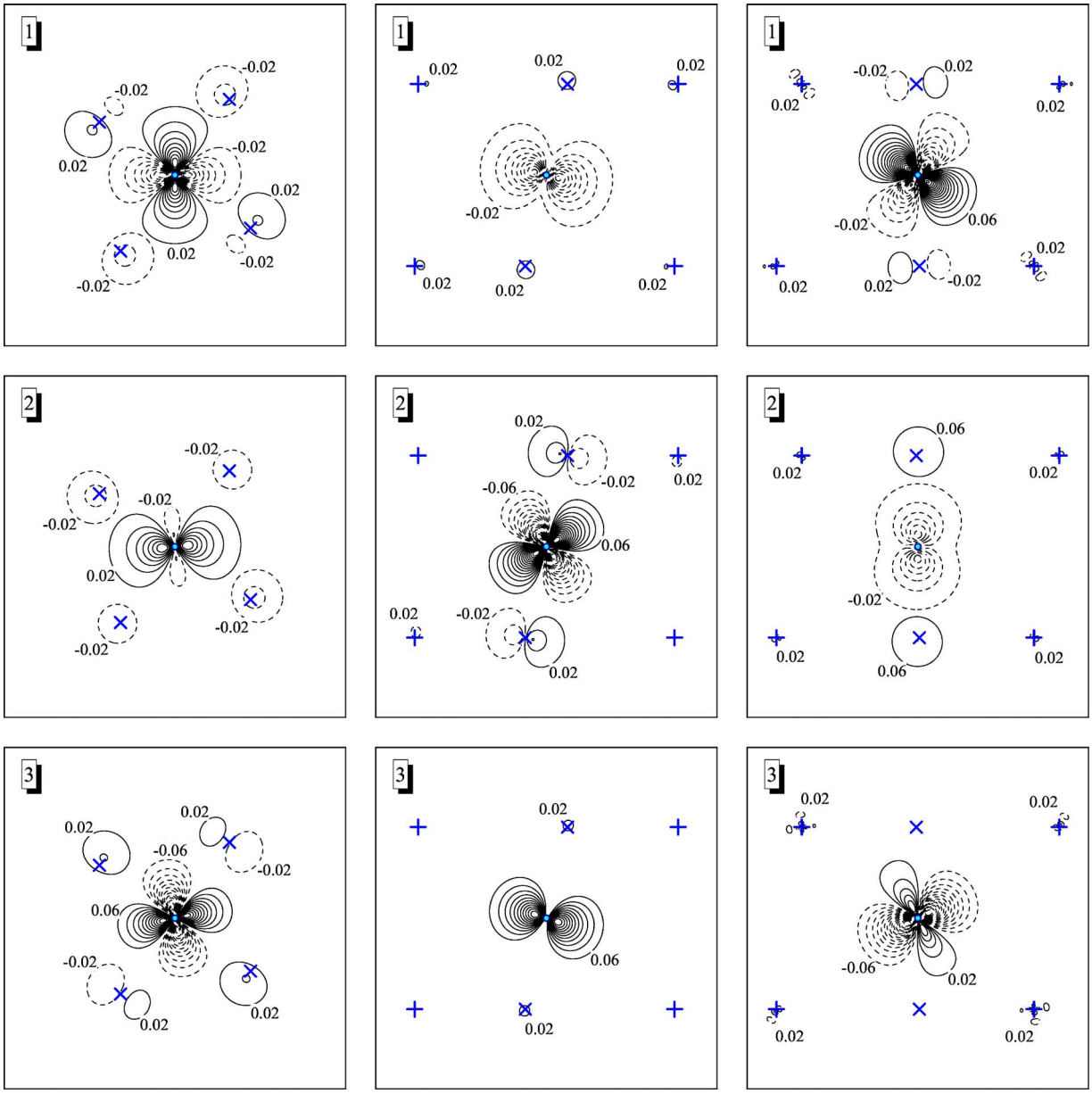

FIG. 3. (Color online) Contour plot of Wannier functions for $LaTiO_3$, in three orthorhombic planes: **ab** (left), **ac** (center), and **bc** (right). The solid and dashed lines correspond to the positive and negative values of the Wannier functions. The projections of different atoms on the planes are denoted by the following symbols: + (La), ○ (Ti), and × (O). Around each atomic site, the Wannier function increases or decreases with the step 0.04 from the values indicated on the graph.

certain set of parameters $\{h^{\alpha\beta}_{\mathbf{RR}'}\}$. The Wannier functions $\{\tilde{W}^{\alpha}_{\mathbf{R}}\}$ for the isolated t_{2g} bands can be obtained from $\{h^{\alpha\beta}_{\mathbf{RR}'}\}$ using the definition $h^{\alpha\beta}_{\mathbf{RR}'}=\langle\tilde{W}^{\alpha}_{\mathbf{R}}|\hat{H}^{\mathrm{LDA}}|\tilde{W}^{\beta}_{\mathbf{R}'}\rangle$, where $\hat{H}^{\mathrm{LDA}}$ is the LDA Hamiltonian in the atomic-spheres approximation.[38]

The (characteristic) example of such Wannier functions constructed for $LaTiO_3$ is shown in Fig. 3, and their extension in the real space is illustrated in Fig. 4. The functions are well localized: about 80–85% of their total weight is accumulated at the central Ti site, 5–9% belong to neighboring oxygen sites, and about 10% is distributed over La, Ti, and O sites located in next coordination spheres. Another measure of localization of the Wannier functions is the expectation value of the square of the position operator, $\langle\mathbf{r}^2\rangle_{\alpha}=\langle\tilde{W}^{\alpha}_{\mathbf{R}}|(\mathbf{r}-\mathbf{R})^2|\tilde{W}^{\alpha}_{\mathbf{R}}\rangle$,[39] which yields $\langle\mathbf{r}^2\rangle_{\alpha}$= 2.68, 2.36, and 2.37 Å^2 for α= 1, 2, and 3, respectively. The Wannier functions for $LaTiO_3$ are less localized in comparison with the more distorted $YTiO_3$, where $\langle\mathbf{r}^2\rangle$ is of the order of 1.90–2.28 Å^2.[34] However, this is to be expected.

The parameters $\{h^{\alpha\beta}_{\mathbf{RR}'}\}$ include all kinds of hybridization (or covalent mixing) effects between transition-metal t_{2g} and other atomic orbitals. However, there are other effects, which are not yet included in $\{h^{\alpha\beta}_{\mathbf{RR}'}\}$. They come from the nonsphericity (NS) of the Madelung potential for the electron-ion interactions, and contribute to the CF splitting. The proper corrections to $\{h^{\alpha\beta}_{\mathbf{RR}'}\}$ can be easily calculated in the basis of Wannier functions $\{\tilde{W}^{\alpha}_{\mathbf{R}}\}$ as

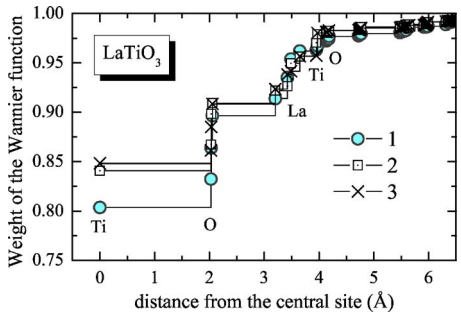

FIG. 4. (Color online) Spacial extension of the Wannier functions in the case of $LaTiO_3$: the weight of the Wannier function accumulated around the central Ti site after adding every new sphere of neighboring atomic sites (also denoted as the "accumulated charge" in Ref. 34).

$$\Delta^{\mathrm{NS}} h^{\alpha\beta}_{\mathbf{RR}} = \sum_{\mathbf{R}' \neq \mathbf{R}} \langle \tilde{W}^{\alpha}_{\mathbf{R}} | \frac{-Z^{*}_{\mathbf{R}'} e^2}{|\mathbf{R} + \mathbf{r} - \mathbf{R}'|} | \tilde{W}^{\beta}_{\mathbf{R}} \rangle, \tag{2}$$

where $Z^{*}_{\mathbf{R}'}$ is the total charge associated with the site $\mathbf{R}'$ (namely, the nuclear charge minus the screening electronic charge encircled by the atomic sphere), and $\mathbf{r}$ is the position of the electron in the sphere $\mathbf{R}$.

The main idea behind this treatment of the CF splitting is based on certain hierarchy of interactions in solids. It implies that the strongest interaction, which leads to the energetic separation of the t_{2g} band from other bands (Fig. 1), is the covalent mixing. For example, in many transition-metal oxides this interaction is mainly responsible for the famous splitting between the transition-metal t_{2g} and e_g states.[40] The nonsphericity of the Madelung potential is considerably weaker than this splitting. However, it can be comparable with the effects of the covalent mixing in the narrow t_{2g} bands. Therefore, the basic idea is to treat this nonsphericity as a pseudoperturbation,[37] and calculate the matrix elements of the Madelung potential in the basis of Wannier functions constructed for spherically averaged ASA potential.

The same strategy can be used for the spin-orbit (SO) interaction, which yields the following correction to the kinetic-energy part of the model Hamiltonian:

$$\Delta^{\mathrm{SO}} h^{\alpha\beta}_{\mathbf{RR}} = \langle \tilde{W}^{\alpha}_{\mathbf{R}} | \frac{\hbar}{4m^2c^2} (\nabla V \times \mathbf{p}) \cdot \boldsymbol{\sigma} | \tilde{W}^{\alpha}_{\mathbf{R}} \rangle$$

(where V is the self-consistent LDA potential and $\boldsymbol{\sigma}$ is the vector of Pauli matrices).

One of the most controversial issues, which is actively discussed in this field, is the magnitude and the direction of the CF splitting in the distorted t_{2g} perovskite oxides. Therefore, we would like to discuss this problem more in details. Basically, there are two sources of discrepancies, which largely affect the conclusions about the orbital ordering and the magnetic ground state.

(1) (The origin of the CF splitting: the nonsphericity of the Madelung potential versus the covalent mixing.) The importance of nonsphericity of the Madelung potential has been emphasized by several authors. The original idea is due to Mochizuki and Imada, who considered the t_{2g}-level splitting in titanites associated with the displacements of the Y and La atoms.[23] It was paraphrased by Cwik *et al.*,[12] who suggested the main effect comes from the deformation of the TiO_6 octahedra. A more general picture has been considered by Schmitz *et al.*,[24] who summed up all contributions in the Madelung potential. A weak point of all these works is an approximate treatment of the covalent mixing (or the hybridization effects), which largely relied on the model parameters. Moreover, the conclusions are sensitive to the value of the dielectric constant, which was treated as an adjustable parameter. On the other hand, the parameters of model Hamiltonian extracted from the first-principles electronic structure calculations using either downfolding (Refs. 28, 30, and 31) or Wannier function (Ref. 32) methods automatically include all effects of the covalent mixing. In this sense, these are more rigorous techniques. However, these calculations were supplemented with the additional atomic-spheres approximation and neglected the nonspherical part of the Madelung potential. This term has been also neglected in our previous work (Ref. 28). As we shall see in Secs. V B and V D, it will definitely revise several statements of Ref. 28. However, the final conclusion about the type of the magnetic ground state of $YTiO_3$ and $LaTiO_3$ appears to be correct.

(2) (The nonuniqueness of the Wannier functions.) Different calculations yield rather different parameters of the CF splitting. For example, for $LaTiO_3$ different authors reported the following values of the CF splitting (between lowest and highest t_{2g} levels): 93 meV (Ref. 28), 200 meV (Ref. 30), and 270 meV (Ref. 32). There is a particularly bad custom to criticize Ref. 28,[24,32,41] which reports the smallest value of the CF splitting, even with certain hints at the accuracy of calculations.[32] It is also premature to think that the small CF splitting will automatically lead to the realization of the orbital liquid state,[20,32] because other model parameters (such as transfer integrals and Coulomb interactions) are also affected by the lattice distortion, which makes a big difference from idealized cubic perovskites.[34]

First, we would like to consider the second part of problem and argue that different values of the CF splitting are most likely related with the different choice of the Wannier functions, which by no means is unique. This is *not* a problem of accuracy of calculations.

In the downfolding method employed in Ref. 28 (and apparently in Refs. 30 and 31), all basis functions have been divided in two groups: the "t_{2g}" part $\{\tilde{\chi}_t\}$, and the "rest" $\{\tilde{\chi}_r\}$. The effective Hamiltonian is constructed by eliminating the "rest" part.[34] A similar idea (although formulated in a different way) has been employed in the projector-operator method,[32] where $\{\tilde{\chi}_t\}$ played a role of trial orbitals for the construction of the Wannier functions. The basic difficulty here is that, in the distorted perovskites, the set of atomic "t_{2g}" orbitals cannot be defined in a unique way: since the local symmetry is not cubic, the abbreviations like "t_{2g}" and "e_g" will always reflect some bad quantum numbers for the states, which are mixed by the crystal field and/or the transfer integrals. In the numerical calculations, the set of "t_{2g}" orbitals is always specified in some local coordinate frame, and the choice of this frame appeared to be different in different calculations. For example, Pavarini *et al.* (Refs. 30 and 31) and Streltsov *et al.* (Ref. 32) selected their local coordi-

nate frames from some geometrical considerations. A completely different strategy has been pursued by the present author, who found the atomic "t_{2g}" orbitals from the diagonalization of the local density matrix.[28]

Then, we are ready to argue that the different choice of the local coordinate frame naturally explains the difference in the parameters of the CF splitting reported by different authors. For these purposes we consider two different setups in the downfolding method, and use $LaTiO_3$ as an example. The first scheme is absolutely identical to the one proposed in Ref. 28, and where the atomic "t_{2g}" orbitals have been defined as three most populated orbitals obtained from the diagonalization of the local density matrix constructed from the t_{2g} bands. In the second scheme, we first construct a more general 40×40 tight-binding Hamiltonian, comprising the Ti($3d$) and La($5d$) states, and reproducing the behavior of 40 overlapping Ti($3d$)-La($5d$) bands. Other orbitals have been eliminated using the downfolding method. Then, we diagonalize the site-diagonal part of this Hamiltonian and associate three lowest eigenstates at each Ti site with the atomic "t_{2g}" orbitals. After that we eliminate the rest of the Ti($3d$) and La($5d$) states using the downfolding method and obtain the minimal 12×12 Hamiltonian for the t_{2g} bands.

Both downfolding schemes are nearly perfect and well reproduce the behavior of t_{2g} bands in the reciprocal space (Fig. 5). However, they yield very different parameters after the Fourier transformation to the real space. For example, the splitting of atomic t_{2g} levels (in meV) obtained in the schemes I and II is (−49, 4, 44) and (−320, 123, 197), respectively. Moreover, the eigenvectors corresponding to the lowest "t_{2g}" levels appear to be also different. In the orthorhombic coordinate frame, specified by the vectors **a**, **b**, and **c**, these eigenvectors have the following form (referred to the site 1): $|\Psi_{\mathrm{I}}\rangle=0.32|xy\rangle-0.73|yz\rangle-0.10|z^2\rangle-0.18|zx\rangle+0.57|x^2-y^2\rangle$ and $|\Psi_{\mathrm{II}}\rangle=0.31|xy\rangle-0.20|yz\rangle+0.15|z^2\rangle+0.55|zx\rangle+0.73|x^2-y^2\rangle$, for the schemes I and II, respectively. Thus, the small value of the CF splitting reported in Ref. 28 is related with the particular choice of the Wannier functions (which is controlled by the parameters of the downfolding scheme). Had we changed our definition of the local coordinate frame, our conclusion would have been also different, and we could easily obtain the CF splitting of the order of 500 meV (and even larger).

Then, it is of course right to ask which scheme is better? In principle, the physics should not depend on the choice of the Wannier functions, and as long as we are dealing only with the kinetic-energy part of the model Hamiltonian, both schemes are totally equivalent as they equally well reproduce the behavior of twelve t_{2g} bands. However, what we want to do next is to combine this kinetic-energy part with the Coulomb interactions, and *to use only the site-diagonal part of these interactions*. This is of course an approximation, and in order to justify this approximation one should guarantee that the Wannier functions, which are used as the basis for the matrix elements of these Coulomb interactions, were sufficiently well localized in the real space, so that all intersite interactions could be neglected.

The degree of localization of the Wannier orbitals is related with the spread of the transfer integrals. Loosely speaking, in order to contribute to the transfer integral between Nth neighbors, the Wannier function should have a finite weight at this neighbor. The distance dependence of transfer integrals calculated for two different schemes is shown in Fig. 5. One can clearly see that the transfer integrals obtained in the scheme I are indeed well localized and basically re-

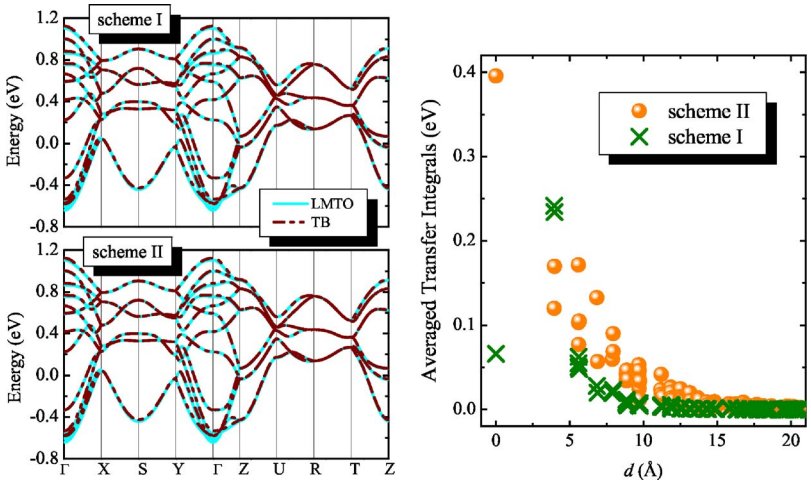

FIG. 5. (Color online) Left panel shows LDA energy bands for $LaTiO_3$ obtained in LMTO calculations and after the tight-binding (TB) parametrization using two different schemes of the downfolding method. In the scheme I, the local coordinate frame has been obtained from the diagonalization of the local density matrix. In the scheme II, the local coordinate frame has been obtained from the diagonalization of the site-diagonal part of a more general 40×40 Ti($3d$)-La($5d$) tight-binding Hamiltonian. Notations of the high-symmetry points of the Brillouin zone are taken from Ref. 42. Right panel shows distance dependence of averaged parameters of the kinetic energy $\bar{h}_{\mathbf{RR}'}(d)=(\Sigma_{\alpha\beta}h^{\alpha\beta}_{\mathbf{RR}'}h^{\beta\alpha}_{\mathbf{R}'\mathbf{R}})^{1/2}$, where d is the distance between transition-metal sites **R** and **R′**. The data for $d=0$ correspond to the crystal-field splitting of the covalent type, and $d\sim4$ Å is the distance between nearest transition-metal sites. Two schemes generate very similar electronic structure in the reciprocal space, which is well consistent with results of original LMTO calculations. However, the real-space parameters appear to be different. The scheme II yields larger crystal-field splitting. However, the transfer integrals are less localized and spread beyond the nearest neighbors.

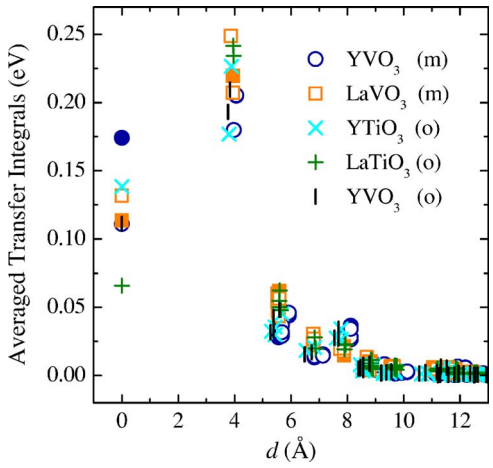

FIG. 6. (Color online) Distance dependence of averaged parameters of the kinetic energy for various compounds. In the orthorhombic (o) structure, all sublattices of the transition-metal sites are equivalent and shown by a single symbol. In the monoclinic (m) structure, the results obtained for two different sublattices are shown by closed and open symbols. For other notations, see Fig. 5.

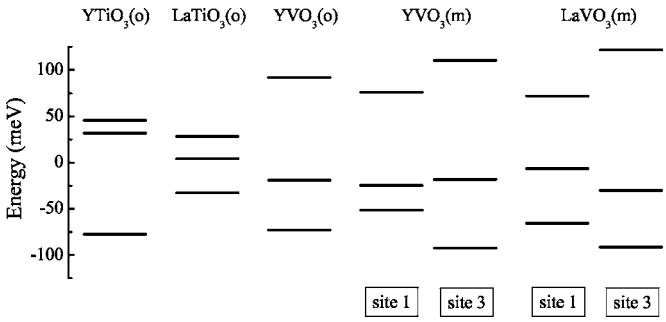

FIG. 8. Summary of the t_{2g}-level splitting in various compounds. The notations "site 1" and "site 3" correspond to two nonequivalent transition-metal sites in the monoclinic phase (shown in Fig. 2).

stricted by the nearest neighbors. The transfer integrals obtained in the scheme II are less localized and spread far beyond the nearest neighbors. Therefore, the Wannier functions, corresponding to the scheme I, should be more localized. This is not surprising, because the scheme I guarantees that the density matrix (or the integrated density of states) at the transition-metal site is well described by the central parts (or by the "heads") of the Wannier functions, given by the atomic orbitals $\{\tilde{\chi}_t\}$.[34] Therefore, the tails of the Wannier functions, coming from the neighboring sites, should be small and largely cancel each other. In the scheme II, the local density matrix is composed both from the "heads" of the Wannier functions and from the tails coming from the neighboring sites. Intuitively, this means that the tail part of the Wannier functions is larger for the scheme II and these functions are less localized.

Thus, we believe that the scheme I is more suitable for the purposes of our work and we apply it to all perovskites. The transfer integrals, obtained in this scheme, are indeed well localized and restricted by the nearest neighbors for all t_{2g} compounds (Fig. 6).

The next important contribution to the CF splitting arises from the nonsphericity of the Madelung potential. This effect is *comparable* with the CF splitting of the covalent type. We have also found that there are several different contributions to the CF splitting, which tend to cancel each other. For example, the CF splitting of the covalent type in $YTiO_3$ and $LaTiO_3$ is largely compensated by the nonsphericity of the Madelung potential originating from the region close to the transition-metal sites and including the neighboring oxygen sites (the cutoff radius $d \sim 2$ Å in Fig. 7).[43] The next important contribution comes from the Y/La and Ti sites, located in the next coordination spheres ($d \sim 4$ Å). In some compounds, even longer-range interactions spreading up to $d \sim 10$ Å can contribute to the sum (2).

The final scheme of the "t_{2g}"-level splitting, which include all these effects, is shown in Fig. 8. The splitting is not particularly large. Nevertheless, as we shall see below, it greatly facilitates the analysis of possible orbital and spin magnetic structures and allows us to explain the type of the magnetic ground state *in all considered compounds*, *except* $LaTiO_3$. The Madelung potential changes not only the magnitude of the crystal-field splitting, but also the form of the atomic "t_{2g}" orbitals, which are split off by the distortion (Table I). These orbitals should predetermine the type of the magnetic ground state in the limit of large Coulomb interactions.

Finally, both form and magnitude of the CF splitting appear to be different for the nonequivalent transition-metal sites in the monoclinic structure. Therefore, one can generally expect rather different behavior of spin and orbital degrees of freedom in two adjacent **ab** planes of the monoclinic phase.

B. Effective Coulomb interactions

The effective Coulomb interactions in the t_{2g} band are defined as the energy cost for moving an electron between

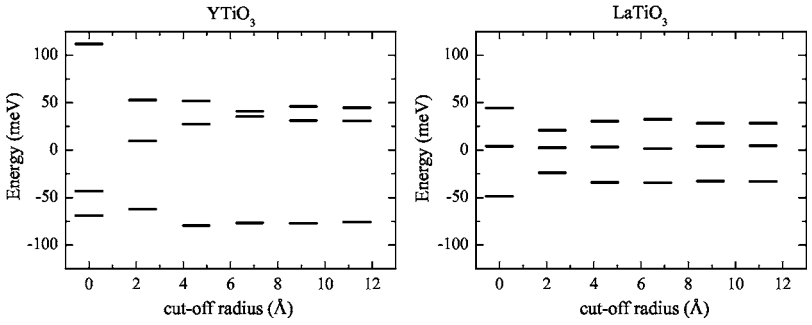

FIG. 7. Convergence of the crystal-field splitting as the function of the cutoff radius for the real-space summation in Eq. (2).

TABLE I. Lowest (for $YTiO_3$ and $LaTiO_3$) and highest (for YVO_3 and $LaVO_3$) atomic orbital obtained from the diagonalization of the site-diagonal part of the model Hamiltonian in the downfolding method (denoted as "covalent part") and after including the nonsphericity of the Madelung potential (denoted as "total"). The symbols o and m stand for orthorhombic and monoclinic phases, respectively. The order of the basis orbitals is xy, yz, z^2, zx, and x^2-y^2, referred to the orthorhombic coordinate frame. The positions of the transition-metal sites are shown in Fig. 2.

Compound	Phase	Site	Covalent part					Total				
$YTiO_3$	o	1	(0.32,	0.78,	0.36,	−0.33,	−0.22)	(−0.13,	0.45,	0.38,	−0.61,	0.50)
$LaTiO_3$	o	1	(−0.32,	0.73,	0.10,	0.18,	−0.57)	(−0.06,	0.85,	0.15,	0.34,	0.37)
YVO_3	o	1	(0.04,	0.84,	0.19,	−0.22,	0.47)	(0.29,	0.90,	0.25,	−0.22,	−0.06)
YVO_3	m	1	(−0.04,	0.47,	0.19,	−0.61,	0.60)	(0.12,	0.54,	0.18,	−0.74,	0.33)
		3	(−0.01,	0.04,	−0.09,	0.79,	0.60)	(0.28,	0.24,	−0.28,	0.89,	−0.05)
$LaVO_3$	m	1	(0.04,	−0.31,	0.11,	0.80,	−0.49)	(0.16,	0.09,	0.01,	0.98,	−0.04)
		3	(−0.01,	0.37,	0.10,	0.75,	0.54)	(−0.09,	0.55,	0.14,	0.78,	0.24)

two Wannier orbitals, $\tilde{W}^{\alpha}_{\mathbf{R}}$ and $\tilde{W}^{\beta}_{\mathbf{R}'}$, which have been initially populated by $\mathfrak{n}_{\mathbf{R}\alpha}$ and $\mathfrak{n}_{\mathbf{R}'\beta}$ electrons,

$$U_{\alpha\alpha\beta\beta} = E[\mathfrak{n}_{\mathbf{R}\alpha}+1, \mathfrak{n}_{\mathbf{R}'\beta}-1] - E[\mathfrak{n}_{\mathbf{R}\alpha}, \mathfrak{n}_{\mathbf{R}'\beta}]. \tag{3}$$

If $\mathbf{R} \neq \mathbf{R}'$, the above matrix elements define the on-site Coulomb interactions, which are screened by intersite interactions. The latter are typically small for the t_{2g} perovskite oxides, and can be neglected in the first approximation.[34] The terms corresponding to $\mathbf{R}=\mathbf{R}'$ define the intra-atomic exchange and nonsphericity of the Coulomb interactions, which are responsible for Hund's rules. More generally, one can consider the transfer of an electron from any linear combination of the Wannier orbitals at the site $\mathbf{R}'$ to any linear combination at the site $\mathbf{R}$. This defines the full matrix of screened Coulomb interactions $\hat{U}=\|U_{\alpha\beta\gamma\delta}\|$. It can be calculated under certain approximations, which have been discussed in details in Ref. 34. The method consists of two parts.

(1) First, we perform the standard constraint-LDA (c-LDA) calculations and artificially switch off all matrix elements of hybridization involving the atomic $3d$ states.[44] This part takes into account the screening of Coulomb interactions caused by the relaxation of the $3d$-atomic basis functions and the redistribution of the rest of the charge density caused by the change of the Coulomb potential. Typical values of on-site Coulomb interactions (u) obtained in this approach vary from 8.5 eV (for titanites) to 9.3 eV (for vanadates). Using the same type of approximations, one can also calculate the intra-atomic exchange coupling constant (j), which is about 0.9 eV for all t_{2g} perovskite oxides. Then, using only u and j, one can restore the full $5\times5\times5\times5$ matrix $\hat{u}\equiv\|u_{\alpha\beta\gamma\delta}\|$ of screened Coulomb interactions between atomic $3d$ orbitals with the same spin, as it is typically done in the LDA+U method.[3]

(2) As the next step, we switch on the hybridization between the atomic $3d$ orbitals and the rest of the basis states, and evaluate the static screening caused by the change of this hybridization in the random-phase approximation (RPA),

$$\hat{U} = [1 - \hat{u}\hat{P}(0)]^{-1}\hat{u}. \tag{4}$$

This scheme implies that different channels of screening can be included consecutively. Namely, the $\hat{u}$ matrix derived from c-LDA is used as the bare Coulomb interaction in the Dyson equation (4), and the $5\times5\times5\times5$ polarization matrix $\hat{P}\equiv\|P_{\alpha\beta\gamma\delta}\|$ describes solely the effects of hybridization of the transition-metal $3d$ states with O($2p$), and either Y($4d$) or La($5d$) states, which lead to the formation of the distinct oxygen $2p$, transition-metal t_{2g}, and a hybrid e_g band shown in Fig. 1. Then, the matrix elements of the polarization function are given by

$$P_{\alpha\beta\gamma\delta}(\omega) = \sum_{n\mathbf{k}}\sum_{n'\mathbf{k}'} \frac{(\mathfrak{n}_{n\mathbf{k}} - \mathfrak{n}_{n'\mathbf{k}'}) d^{\dagger}_{\alpha n'\mathbf{k}'} d_{\beta n\mathbf{k}} d^{\dagger}_{\gamma n\mathbf{k}} d_{\delta n'\mathbf{k}'}}{\omega - \varepsilon_{n'\mathbf{k}'} + \varepsilon_{n\mathbf{k}} + i\delta(\mathfrak{n}_{n\mathbf{k}} - \mathfrak{n}_{n'\mathbf{k}'})}, \tag{5}$$

where $\{\varepsilon_{n\mathbf{k}}\}$ and $\{\mathfrak{n}_{n\mathbf{k}}\}$ are LDA eigenvalues and occupation numbers for the band n and momentum $\mathbf{k}$ in the first Brillouin zone (the spin index is already included in the definition of n) and $d_{\gamma n\mathbf{k}}=\langle\tilde{\chi}_{\gamma}|\psi_{n\mathbf{k}}\rangle$ is the projection of LDA eigenstate $\psi_{n\mathbf{k}}$ onto the atomic $3d$ orbital $\tilde{\chi}_{\gamma}$. Note that in order to calculate $\hat{P}$, we use the electronic structure obtained in the local-density approximation, which yields an incorrect metallic behavior for all considered compounds. Therefore, in the process of calculation of the screened Coulomb interaction, we should get rid of the parasitic metallic screening. This is typically done by switching off all transitions between t_{2g} bands in the polarization function (5).[5,34] Therefore, when we employ the HF approximation for the solution of our model Hamiltonian (1), this means that we take into account all channels of screening, except the self-screening by the t_{2g} electrons (that is totally in spirit of the HF approximation). The screening by the t_{2g} electrons can be included by considering the correlation effects beyond the HF approximation.[5] However, the result of such screening will be clearly different from RPA screening for the metallic t_{2g} bands in the local-density approximation.

Hence, we obtain a $5\times5\times5\times5$ matrix of screened Coulomb interactions in the basis of all five $3d$ orbitals. This matrix is transformed to the local coordinate frame spanned

TABLE II. Results of fitting of the effective Coulomb interactions in the t_{2g} band obtained in the hybrid c-LDA+RPA approach in terms of two Kanamori parameters: the intraorbital Coulomb interaction $\mathcal{U}$ and the exchange interaction $\mathcal{J}$ (in eV) (Refs. 45 and 46). The symbols o and m stand for the orthorhombic and monoclinic phases, respectively. The positions of the transition-metal sites are shown in Fig. 2.

Compound	Phase	Site	$\mathcal{U}$	$\mathcal{J}$
$YTiO_3$	o	1	3.45	0.62
$LaTiO_3$	o	1	3.20	0.61
YVO_3	o	1	3.27	0.63
YVO_3	m	1	3.19	0.63
		3	3.26	0.63
$LaVO_3$	m	1	3.11	0.62
		3	3.12	0.62

by only three "t_{2g}" orbitals with the same spin. The obtained $3\times3\times3\times3$ matrix is expanded in the spin subspace using the orthogonality condition between Wannier orbitals with different spins. This yields a $6\times6\times6\times6$ matrix $\hat{U}$, which was used in the actual calculations.

Only for explanatory purposes, we fit $\hat{U}$ in terms of two Kanamori parameters: the intraorbital Coulomb interaction $\mathcal{U}$ and the intra-atomic exchange interaction $\mathcal{J}$.[45,46] The results of such fitting are shown in Table II. There is the clear dependence of the parameter $\mathcal{U}$ on the local environment in solid, which is captured by the RPA calculations.[34] Generally, the value of $\mathcal{U}$ is larger for more distorted Y compounds. There is also a clear correlation between the value of $\mathcal{U}$ and the magnitude of the local distortion around two nonequivalent transition-metal sites in the monoclinic phase: the sites experiencing larger distortion (according to the magnitude of the CF splitting in Fig. 8) have larger $\mathcal{U}$. On the other hand, $\mathcal{J}$ is practically insensitive to the local environment in solids.

It is important to note that our values of the effective Coulomb interactions $\mathcal{U}$ are considerably smaller than experimental Kanamori parameters for the transition-metal oxides, which are typically derived from the analysis of photoemission spectra.[19,47] To a smaller extent, the same apply to the parameters of intra-atomic exchange interactions $\mathcal{J}$. However, this is to be expected. Note that the photoemission spectra are typically interpreted in the cluster model, which treats *explicitly* all transition-metal $3d$ and oxygen $2p$ states. However, in our model we want to keep only the transition-metal t_{2g} bands and include the effect of other states *implicitly*, i.e., through the renormalization of the interaction parameters in the t_{2g} band. Therefore, our parameters should be generally smaller than in the cluster model. For example, the transfer of an electron, associated with the reaction (3) will cause the change of the electronic structure in the oxygen $2p$ and transition-metal e_g bands (see Fig. 1), which tends to compensate the change of the number of t_{2g} electrons at different transition-metal sites. Since the oxygen $2p$ and transition-metal e_g bands are eliminated in our t_{2g} model, this change of the electronic structure should be effectively included into the screening of Coulomb and exchange interactions in the t_{2g} band. In practical calculations, this effect is taken into account through the RPA channel of screening.[34]

IV. SOLUTION OF MODEL HAMILTONIAN

In this section we briefly discuss the methods of solution of the model Hamiltonian (1). We start with the simplest HF approach, which totally neglects the correlation effects. Then, we consider two simple corrections to the HF approximation, which will allow us to include some of these effects. One is the second-order perturbation theory for the total energy. It shares common problems of the regular (nondegenerate) perturbation theory and allows us to calculate easily the correction to the total energy, starting from the single-Slater-determinant approximation for the many-electron wave functions. Therefore, we expect this method to work well for the systems where the orbital degeneracy is already lifted and the ground state is described reasonably well by a single Slater determinant, so that other corrections can be treated as a perturbation. The second scheme is the variational superexchange theory for d^1 perovskites (titanites), which takes into account the multiplet structure of the excited atomic states. It will allow us to study the effect of electron correlations on the orbital ordering. However, it is limited by typical approximations made in the theory of superexchange interactions, which treat all transfer integrals as a perturbation.

All calculations have been performed in the basis of Wannier functions $\{\tilde{W}^{\alpha}_{\mathbf{R}}\}$, which have a finite weight at the central transition-metal site as well as the oxygen and other atomic sites located in its neighborhood. In order to calculate the local quantities, associated with the transition-metal atoms, such as spin and orbital magnetic moments as well as the distribution of the charge density, the Wannier functions have been expanded over the standard LMTO basis functions, and the aforementioned quantities have been obtained after radial integration over atomic spheres of the transition-metal sites.

A. Hartree-Fock approximation

The Hartree-Fock approximation provides the simplest solution of the many-body problem described by the model Hamiltonian (1). In this case, the trial wave function for the many-electron ground state is searched in the form of a single Slater determinant $|S\{\varphi_{n\mathbf{k}}\}\rangle$, which is constructed from the one-electron orbitals $\{\varphi_{n\mathbf{k}}\}$. The latter are subjected to the variational principle and requested to minimize the total energy

$$E_{\mathrm{HF}} = \min_{\{\varphi_{n\mathbf{k}}\}} \langle S\{\varphi_{n\mathbf{k}}\}|\hat{\mathcal{H}}|S\{\varphi_{n\mathbf{k}}\}\rangle$$

for a given number of particles $\mathcal{N}$, yielding the set of well-known HF equations,

$$(\hat{h}_{\mathbf{k}} + \hat{V})|\varphi_{n\mathbf{k}}\rangle = \varepsilon_{n\mathbf{k}}|\varphi_{n\mathbf{k}}\rangle, \tag{6}$$

where $\hat{h}_{\mathbf{k}} \equiv \|h^{\alpha\beta}_{\mathbf{k}}\|$ is the kinetic part of the model Hamiltonian (1) in the reciprocal space: $h^{\alpha\beta}_{\mathbf{k}} = \frac{1}{N}\Sigma_{\mathbf{R}'} h^{\alpha\beta}_{\mathbf{RR}'} e^{-i\mathbf{k}\cdot(\mathbf{R}-\mathbf{R}')}$ (N being the number of sites), and $\hat{V} \equiv \|V_{\alpha\beta}\|$ is the HF potential,

$$V_{\alpha\beta} = \sum_{\gamma\delta} (U_{\alpha\beta\gamma\delta} - U_{\alpha\delta\gamma\beta}) n_{\gamma\delta}. \quad (7)$$

Again, for the sake of simplicity of our notations, we drop here the dependence of $V_{\alpha\beta}$ on the index $\mathbf{R}$. Equation (6) is solved self-consistently together with the equation

$$\hat{n} = \sum_{n\mathbf{k}}^{\text{occ}} |\varphi_{n\mathbf{k}}\rangle\langle\varphi_{n\mathbf{k}}|$$

for the density matrix $\hat{n} \equiv \|n_{\alpha\beta}\|$ in the basis of Wannier orbitals.

After the self-consistency, the total energy can be calculated as

$$E_{\text{HF}} = \sum_{n\mathbf{k}}^{\text{occ}} \varepsilon_{n\mathbf{k}} - \frac{1}{2}\sum_{\alpha\beta} V_{\beta\alpha} n_{\alpha\beta}.$$

Using $\{\varepsilon_{n\mathbf{k}}\}$ and $\{\varphi_{n\mathbf{k}}\}$, one can also calculate the one-electron Green function

$$\hat{\mathcal{G}}_{\mathbf{RR}'}(\omega) = \sum_{n\mathbf{k}} \frac{|\varphi_{n\mathbf{k}}\rangle\langle\varphi_{n\mathbf{k}}|}{\omega - \varepsilon_{n\mathbf{k}} + i\delta} e^{i\mathbf{k}\cdot(\mathbf{R}-\mathbf{R}')}.$$

The latter is widely used for the analysis of interatomic magnetic interactions,[48]

$$J_{\mathbf{RR}'} = \frac{1}{2\pi} \text{Im} \int_{-\infty}^{\varepsilon_{\text{F}}} d\varepsilon \, \text{Tr}_L[\hat{\mathcal{G}}^{\uparrow}_{\mathbf{RR}'}(\omega)\Delta\hat{V}\hat{\mathcal{G}}^{\downarrow}_{\mathbf{R}'\mathbf{R}}(\omega)\Delta\hat{V}], \quad (8)$$

where $\hat{\mathcal{G}}^{\uparrow,\downarrow}_{\mathbf{RR}'} = \frac{1}{2}\text{Tr}_S[(\hat{1} \pm \hat{\sigma}_z)\hat{\mathcal{G}}_{\mathbf{RR}'}]$ is the projection of the Green function onto the majority ($\uparrow$) and minority ($\downarrow$) spin states, $\Delta\hat{V} = \text{Tr}_S\{\hat{\sigma}_z\hat{V}\}$ is the magnetic (spin) part of the HF potential, Tr_S (Tr_L) denotes the trace over the spin (orbital) indices, $\hat{1}$ and $\hat{\sigma}_z$ are, correspondingly, the unity and Pauli matrices of the dimension 6, and ε_{F} is the Fermi energy.

The interatomic magnetic interactions $\{J_{\mathbf{RR}'}\}$ characterize the spin stiffness of the magnetic phase. Therefore, they can be directly compared with the experimental magnon (spin-wave) spectra derived from inelastic neutron scattering measurements.

According to Eq. (8), $J_{\mathbf{RR}'} > 0$ (< 0) means that for a given magnetic structure, the spin arrangement in the bond $\langle\mathbf{RR}'\rangle$ corresponds to the local minimum (maximum) of the total energy. However, in the following we will use the universal notations, according to which $J_{\mathbf{RR}'} > 0$ and < 0 will stand the ferromagnetic and antiferromagnetic coupling, respectively. This corresponds to the *local mapping* of the HF energies onto the Heisenberg model

$$E_{\text{Heis}} = -\sum_{\langle\mathbf{RR}'\rangle} J_{\mathbf{RR}'} \mathbf{e}_{\mathbf{R}} \cdot \mathbf{e}_{\mathbf{R}'}, \quad (9)$$

where $\mathbf{e}_{\mathbf{R}}$ is the direction of the spin magnetic moment at the site $\mathbf{R}$. The "local mapping" means that, strictly speaking, the total energy change given by Eq. (9) is justified only for infinitesimal rotations of the spin magnetic moment near certain equilibrium state. The results of such mapping near another equilibrium state can be generally different, for example, due to different type of the orbital ordering realized in this state. Therefore, the magnetic interactions can be regarded as the local probe of the orbital ordering in each magnetic state.

B. Second order perturbation theory for correlation energy

The simplest way to go beyond the HF approximation is to include the correlation interactions in the second order of perturbation theory for the total energy.[49] The correlation interaction (or a fluctuation) is defined as the difference between true many-body Hamiltonian (1), and its one-electron counterpart, obtained at the level of HF approximation

$$\hat{\mathcal{H}}_C = \sum_{\mathbf{R}} \left(\frac{1}{2} \sum_{\alpha\beta\gamma\delta} U_{\alpha\beta\gamma\delta} \hat{c}^{\dagger}_{\mathbf{R}\alpha} \hat{c}^{\dagger}_{\mathbf{R}\gamma} \hat{c}_{\mathbf{R}\beta} \hat{c}_{\mathbf{R}\delta} - \sum_{\alpha\beta} V_{\alpha\beta} \hat{c}^{\dagger}_{\mathbf{R}\alpha} \hat{c}_{\mathbf{R}\beta} \right). \quad (10)$$

By treating $\hat{\mathcal{H}}_C$ as a perturbation, the correlation energy can be easily estimated as[49]

$$E_C = -\sum_{S} \frac{\langle G|\hat{\mathcal{H}}_C|S\rangle\langle S|\hat{\mathcal{H}}_C|G\rangle}{E_{\text{HF}}(S) - E_{\text{HF}}(G)}, \quad (11)$$

where $|G\rangle$ and $|S\rangle$ are the Slater determinants corresponding to the low-energy ground state in the HF approximation, and the excited state, respectively. Due to the variational properties of the Hartree-Fock method, the only processes which may contribute to E_C are the two-particle excitations, for which each $|S\rangle$ is obtained from $|G\rangle$ by replacing two one-electron orbitals, say $\varphi_{n_1\mathbf{k}_1}$ and $\varphi_{n_2\mathbf{k}_2}$, from the occupied part of the spectrum by two unoccupied orbitals, say $\varphi_{n_3\mathbf{k}_3}$ and $\varphi_{n_4\mathbf{k}_4}$. Hence, using the notations of Sec. III, the matrix elements take the following form:

$$\langle S|\hat{\mathcal{H}}_C|G\rangle = \langle\varphi_{n_3\mathbf{k}_3}\varphi_{n_4\mathbf{k}_4}|v_{\text{scr}}|\varphi_{n_1\mathbf{k}_1}\varphi_{n_2\mathbf{k}_2}\rangle - \langle\varphi_{n_3\mathbf{k}_3}\varphi_{n_4\mathbf{k}_4}|v_{\text{scr}}|\varphi_{n_2\mathbf{k}_2}\varphi_{n_1\mathbf{k}_1}\rangle. \quad (12)$$

These matrix elements satisfy the following condition: $\langle S|\hat{\mathcal{H}}_C|G\rangle \sim \frac{1}{N}\Sigma_{\mathbf{R}} e^{i(\mathbf{k}_3+\mathbf{k}_4-\mathbf{k}_1-\mathbf{k}_2)\cdot\mathbf{R}}$, provided that the screened Coulomb interactions are diagonal with respect to the site indices. In the following we will retain only the $\mathbf{R}=0$ part in this sum. This corresponds to the single-site approximation for the correlation interactions, which is known to be good for three-dimensional systems and becomes exact in the limit of infinite spacial dimensions.[50]

Finally, we employ a common approximation of noninteracting quasiparticles and replace the denominator of Eq. (11) by the linear combination of HF eigenvalues: $E_{\text{HF}}(S) - E_{\text{HF}}(G) \approx \varepsilon_{n_3\mathbf{k}_3} + \varepsilon_{n_4\mathbf{k}_4} - \varepsilon_{n_1\mathbf{k}_1} - \varepsilon_{n_2\mathbf{k}_2}$.[49]

The form of Eq. (11) implies that the HF ground state is *nondegenerate*, and the correlation effects can be systematically included by considering the regular perturbation theory expansion. It is not applicable for cubic perovskites, where the HF ground state is known to be infinitely degenerate (with respect to different orbital configurations) and the correlation energy should be evaluated on the basis of a *degenerate* perturbation theory.[20] Thus, the use of Eq. (11) implies that the orbital degeneracy is already lifted by the crystal

distortion. As we shall see below, this approximation can be justified for a number of perovskite compounds (although with some exceptions and reservations).

C. Effects of multiplet structure in the theory of superexchange interactions

Another method, which allows us to treat some correlation effects beyond the mean-field HF approximation is the theory of superexchange interactions starting with the correct multiplet structure of the atomic states. Similar idea has been discussed in the context of colossal magnetoresistive manganites (Refs. 51 and 52) and cubic t_{2g} perovskites (Ref. 52). Here we focus mainly on the interplay of superexchange interactions with the lattice distortion. The formulation is extremely simple for the d^1 compounds, like $YTiO_3$ and $LaTiO_3$.

The superexchange interaction in the bond $\langle \mathbf{R}\mathbf{R}' \rangle$ is basically the gain of the kinetic energy, which is acquired by an electron occupying the atomic orbital $\phi_{\mathbf{R}}$ of site $\mathbf{R}$ in the process of virtual hoppings into the subspace of unoccupied states of the (neighboring) site $\mathbf{R}'$, and vice versa.[53,54] In the atomic limit for the d^1 compounds, there is only one t_{2g} electron at each Ti site. This is essentially a one-electron problem, where the form of the atomic orbital $\phi_{\mathbf{R}}$ is determined by the site-diagonal part of the kinetic energy $\|h^{\alpha\beta}_{\mathbf{R}\mathbf{R}}\|$, incorporating the effects of the spin-orbit interaction and the CF splitting. Therefore, in the pure atomic limit, the ground-state wave function for each bond $\langle \mathbf{R}\mathbf{R}' \rangle$ can be taken in the form of a single Slater determinant

$$|G_{\mathbf{R}\mathbf{R}'}\rangle = \frac{1}{\sqrt{2}}[\phi_{\mathbf{R}}(1)\phi_{\mathbf{R}'}(2) - \phi_{\mathbf{R}'}(1)\phi_{\mathbf{R}}(2)].$$

Then, $\phi_{\mathbf{R}}$ and $\phi_{\mathbf{R}'}$ are expanded over the Wannier orbitals associated with the site $\mathbf{R}$ and $\mathbf{R}'$ and the transfer integrals connecting different Wannier orbitals are treated as a perturbation. The excited states at the sites $\mathbf{R}$ and $\mathbf{R}'$, which appear in the process of virtual hoppings are the two-electron states and subjected to the multiplet splitting. This is exactly the point where the electron correlations, beyond the HF approximation, enter the problem. In order to incorporate these effects, we note that from $m=6$ Wannier spin orbitals $\{\tilde{W}^{\alpha}_{\mathbf{R}}\}$ at each Ti site, one can construct $\frac{1}{2}m(m-1)=15$ antisymmetric two-electron Slater's determinants $\{|S\rangle\}$ $(S=1,\ldots,15)$, which can be used as the basis for the screened Coulomb interactions in the excited state: $U_{SS'}=\langle S|v_{\mathrm{scr}}|S'\rangle$. The diagonalization of this 15×15 matrix yields the complete set of eigenvalues $\{E_{\mathbf{R}M}\}$ and eigenfunctions $\{|\mathbf{R}M\rangle\}$ of the two-electron states at the site $\mathbf{R}$ $(M=1,\ldots,15)$. An example of such a multiplet structure for $YTiO_3$ and $LaTiO_3$ is shown in Fig. 9. According to the first Hund rule, the lowest-energy configuration corresponds to the spin-triplet state $^3T_{1g}$. The degeneracy of the $^3T_{1g}$, ^3E_g, and $^3T_{2g}$ levels is lifted by the orthorhombic distortion, which affects the matrix elements of the effective Coulomb interaction via the RPA channel of screening. The splitting is larger for the more distorted $YTiO_3$.

In order to calculate the energy gain caused by the virtual hoppings, the eigenfunctions $\{|\mathbf{R}M\rangle\}$ shall be projected onto

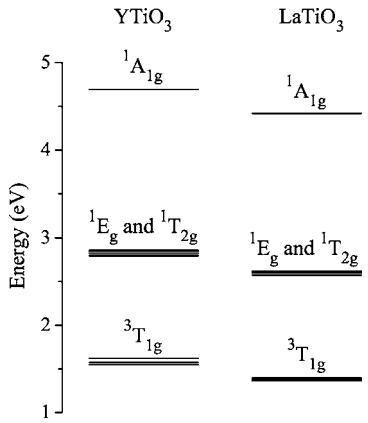

FIG. 9. The multiplet structure of the excited atomic configuration t^2_{2g} in $YTiO_3$ and $LaTiO_3$.

the physical subspace of two-electron states which can be created by transferring an electron from the neighboring sites. The corresponding projector operators have the form $\hat{\mathcal{P}}_{\mathbf{R}}=\Sigma_{\alpha}|P^{\alpha}_{\mathbf{R}}\rangle\langle P^{\alpha}_{\mathbf{R}}|$, where

$$|P^{\alpha}_{\mathbf{R}}\rangle = \tfrac{1}{\sqrt{2}}\{\phi_{\mathbf{R}}(1)\tilde{W}^{\alpha}_{\mathbf{R}}(2) - \tilde{W}^{\alpha}_{\mathbf{R}}(1)\phi_{\mathbf{R}}(2)\}$$

is the Slater determinant constructed from the occupied orbital $\phi_{\mathbf{R}}$ and one of the basis Wannier orbitals $\tilde{W}^{\alpha}_{\mathbf{R}}$. In the other words, the projection $\hat{\mathcal{P}}_{\mathbf{R}}$ imposes an additional constraint, which guarantees that one of the orbitals in the two-electron state must be $\phi_{\mathbf{R}}$. Then, the energy gain caused by the virtual hoppings in the bond $\langle \mathbf{R}\mathbf{R}' \rangle$ is given by

$$\Delta E_{\mathbf{R}\mathbf{R}'} = -\langle G_{\mathbf{R}\mathbf{R}'}|\hat{h}_{\mathbf{R}\mathbf{R}'}\left(\sum_{M}\frac{\hat{\mathcal{P}}_{\mathbf{R}'}|\mathbf{R}'M\rangle\langle\mathbf{R}'M|\hat{\mathcal{P}}_{\mathbf{R}'}}{E_{\mathbf{R}'M}}\right)\hat{h}_{\mathbf{R}'\mathbf{R}} + (\mathbf{R}\leftrightarrow\mathbf{R}')|G_{\mathbf{R}\mathbf{R}'}\rangle. \quad (13)$$

The total energy of the system in the superexchange approximation is obtained after summation over all bonds, which should be combined with the site-diagonal elements, incorporating the effects of the CF splitting and the relativistic spin-orbit interaction:

$$E_{\mathrm{SE}} = \sum_{\mathbf{R}}\langle\phi_{\mathbf{R}}|\hat{h}_{\mathbf{R}\mathbf{R}}|\phi_{\mathbf{R}}\rangle + \sum_{\langle\mathbf{R}\mathbf{R}'\rangle}\Delta E_{\mathbf{R}\mathbf{R}'}.$$

Finally, the set of occupied orbitals $\{\phi_{\mathbf{R}}\}$ is obtained by minimizing E_{SE}, e.g., using the steepest descent method.

For a given orbital ordering, the multiplet effects are expected to be more important in the case of the AFM spin ordering, where an electron comes to the neighboring site with the opposite direction of spin. In this case, the excited configuration is subjected to the multiplet splitting into the spin-singlet and spin-triplet states, which additionally stabilizes the AFM spin state.[55]

V. RESULTS AND DISCUSSIONS

In this section we present results of solution the model Hamiltonian (1) for the distorted perovskite compounds. We

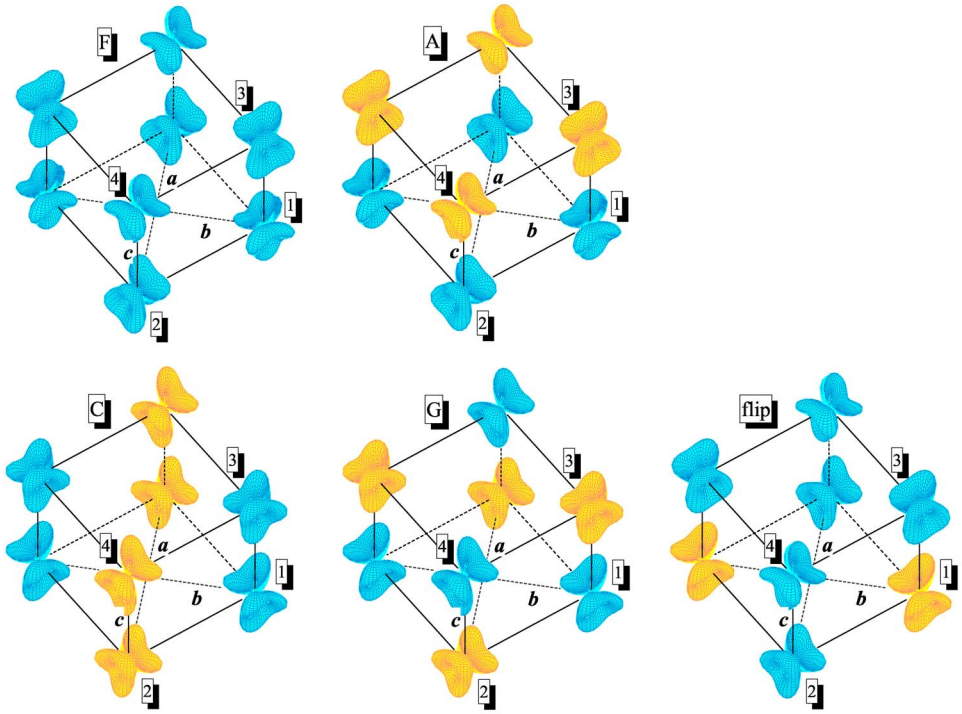

FIG. 10. (Color online) Distribution of the charge density around V sites in various magnetic phases of orthorhombically distorted YVO_3 ($T<77$ K), as obtained in the Hartree-Fock calculations. Different magnetic sublattices are shown by dark gray (blue) and light gray (yellow) colors.

start with Y-based perovskites, where the orbital ordering is largely controlled by the CF splitting coming from the experimental lattice distortion. We will show that this distortion imposes a severe constraint on the magnetic properties and predetermines the type of the magnetic ground state. Then, we will consider the La-based perovskites, where the situation is less clear: while in $LaVO_3$ the experimental distortion largely controls the type of the orbital ordering *in one of the* **ab** *planes*, it is generally small in $LaTiO_3$, that poses many open and unresolved questions.

First, we will consider the effect of the pure crystal distortion, without spin-orbit interaction. The latter will be discussed separately in Sec. V E.

A. YVO_3

YVO_3 exhibits two structural phase transitions.[14,15] The first one is the second-order transition from orthorhombic (D_{2h}^{16}) to monoclinic (apparently D_{2h}^{5}) phase, which takes places at 200 K and is believed to coincide with the onset of the orbital ordering. The second one is the first-order transition at 77 K from monoclinic to another orthorhombic phase. The magnetic transition temperature is 116 K, which lies in the monoclinic region and does not coincide with any structural phase transition. On the other hand, the change of the crystal structure at 77 K coincides with the magnetic phase transition. The magnetic structure in the interval 77 K $<T<$ 116 K is C-type AFM, while below 77 K it becomes G-type AFM.

1. Low-temperature orthorhombic phase ($T<77$ K)

YVO_3 has the largest CF splitting amongst considered orthorhombic perovskite oxides (Fig. 8). It lowers the energies of two t_{2g} levels, which are just enough to accommodate two d electrons. The highest level is separated from the middle one by a 111 meV gap. Therefore, the orbital degrees of freedom in this d^2 compound are expected to be quenched (at least partially) by the crystal distortion.

This is clearly seen in our Hartree-Fock calculations. The orbital ordering depends on the magnetic state. However, this dependence is weak and can be hardly seen on the plot (Fig. 10). The form of the orbital ordering, which can be schematically viewed as an alternation of the (xy,yz) and (xy,zx) orbitals in the cubic coordinate frame associated with the VO_6 octahedra, is in an excellent agreement with the one predicted by Sawada and Terakura on the basis of LDA+U calculations,[27] and which was later on confirmed in synchrotron x-ray-diffraction experiments.[56]

The first important question, which we would like to address here is where does this ordering come from? In Fig. 11 we show results of calculations obtained using three different

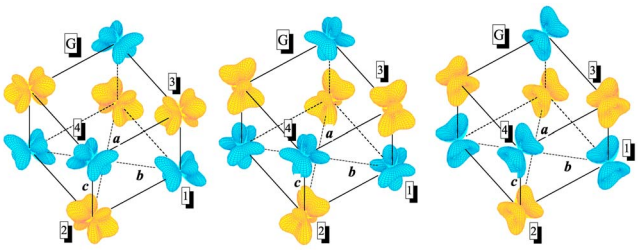

FIG. 11. (Color online) Orbital ordering in the G-type antiferromagnetic phase of orthorhombically distorted YVO_3 computed without crystal field (left), including the crystal field of the covalent type (middle), and the crystal field of both covalent and Madelung type (right).

TABLE III. Magnetic interactions ($J_{\mathbf{RR}'}$), Hartree-Fock energies (E_{HF}), and total energies (E_{tot}) in the orthorhombic phase of YVO_3 ($T<77$ K). The energies are measured from the most stable magnetic state in meV per one formula unit. The magnetic interactions are measured in meV. The total energy is defined as Hartree-Fock energy plus correlation energies (E_C) in the second order of perturbation theory, $E_{\mathrm{tot}}=E_{\mathrm{HF}}+E_C$.

Phase	J_{12}	J_{13}	J_{24}	J_{34}	E_{HF}	E_{tot}
F	−1.4	−3.6	−3.6	−1.4	21.7	27.1
A	−2.5	−3.7	−3.7	−2.5	14.6	17.3
C	−4.7	−4.9	−4.9	−4.7	10.1	11.7
G	−4.4	−4.8	−4.8	−4.4	0	0
Flip	−4.0	−4.8	−3.9	−1.8	11.6	14.0

settings for the site-diagonal part of the kinetic energy: (i) $h^{\alpha\beta}_{\mathbf{RR}}=0$ (i.e., there is no CF splitting at all); (ii) the parameters $\{h^{\alpha\beta}_{\mathbf{RR}}\}$ extracted from the downfolding method, which takes into account only the covalent type of the CF splitting; and (iii) the parameters $\{h^{\alpha\beta}_{\mathbf{RR}}\}$ obtained in the downfolding method and corrected for the nonsphericity of the Madelung potential (2). One can clearly see that in order to reproduce the correct orbital ordering, all contributions to the CF splitting appear to be important. Had we neglected some of these contributions, not only the orbital ordering but also the magnetic ground state would have been different. For example, without the Madelung term, the magnetic ground state is expected to be of the A type, being in clear disagreement with the experimental data.

As it has been already discussed by other authors,[19,27,29] the C-type orbital ordering shown in Fig. 10 favors the G-type AFM spin ordering, which emerges as the ground state already at the level of HF calculations (Table III). The order of the magnetic states, corresponding to the increase of the total energy, is $G\rightarrow C\rightarrow \mathrm{flip}\rightarrow A\rightarrow F$, which is well consistent with results of all-electron LDA+U calculations.[27,29,57]

However, the orbital ordering *is not* fully quenched by the crystal distortion and to certain extent can adjust the change of the magnetic state by further minimizing the energies of superexchange interaction.[54] This is seen particularly well in the behavior of interatomic magnetic interactions, which reveal an appreciable dependence on the magnetic state. For example, by going from the G state to the F state, the in-plane interaction J_{12} (J_{34}) changes by nearly 70%, and the interplane interaction J_{13} (J_{24}) changes by 25%.

In agreement with the experimental finding,[16] the magnetic interactions obtained for the G-type AFM ground state are nearly isotropic. However, this isotropic behavior can be easily destroyed by the small change of the orbital ordering in other magnetic states.

The absolute values of J_{12} and J_{13} for the G-type AFM phase are underestimated by about 1 meV (i.e., by nearly 20%) in comparison with the parameters extracted from the fit of the experimental magnon spectra ($J_{12}=J_{13}=-5.7\pm0.3$ meV). This seems to be reasonable because the HF method is a single-Slater-determinant approach, which does not take into account the correlation effects. The magnitude of the correlation energy depends on the magnetic state and is expected to be larger in the case of the AFM spin alignment, where the net magnetization is zero and the choice of the many-electron wave function in the form of a single Slater determinant is always an approximation.[5] On the other hand, the saturated ferromagnetic state can be described reasonably well by a single Slater determinant (provided that the orbital degeneracy is already lifted by the crystal distortion). All these trends are clearly seen in the total energy calculations, which take into account the correlation effects in the second order of perturbation theory (Table III). The correlations additionally stabilize the G-type AFM ground state relative to other magnetic states. However, it does not change the order of the magnetic states.

The absolute values of the correlation energy obtained for the ferromagnetic and G-type AFM phases of YVO_3 are correspondingly 2 and 7 meV per one formula unit. These are rather typical values for all considered compounds except $LaTiO_3$, where the characteristic correlation energies are substantially larger (see Sec. V D).

Unfortunately, it is not possible to estimates the effect of electron correlations on the interatomic magnetic interactions directly, using Eq. (8). Nevertheless, one can still try to use the total energy differences between different magnetic states and map them onto the Heisenberg model.[58] This is a cruder approximation, which implies that the orbital ordering is completely quenched by the crystal distortion and does not depend on the magnetic state. Although it is not strictly true, we will use this approximation here in order to get a rough idea about the impact of the correlation energy on the parameters of interatomic magnetic interactions. Then, the standard HF approximation yields $J_{12}=-3.3$ meV and $J_{13}=-4.3$ meV, while the second order perturbation theory for the correlation energy yields $J_{12}=-4.1$ meV and $J_{13}=-5.4$ meV. Therefore, the 1 meV difference between parameters of interatomic magnetic interactions obtained in the HF approximation and the experimental magnon data can be naturally attributed to the correlation effects. This example clearly shows that for the detailed analysis of electronic and magnetic properties of t_{2g} perovskite oxides, it is necessary to go beyond the HF approximation and consider the correlation effects.

2. *High-temperature monoclinic phase* (77 K$<T<$116 K)

The monoclinic distortion creates two inequivalent types of V atoms, which lie in different **ab** planes, denoted as (1,2) and (3,4) in Fig. 2. It also changes the scheme of the crystal-field splitting of the atomic t_{2g} levels (Fig. 8). Energetically, the new scheme is rather similar to the previous one, observed in the orthorhombic phase. In both planes it lowers the energies of two t_{2g} levels. The energy gap, which separates the highest level from the middle one is 101 and 128 meV for the sites 1 and 3, respectively. However, the type of the orbitals which are split off by the monoclinic distortion is different (Table I). This leads to the new type of stacking between the planes, which is sometimes referred to as the G-type AFM orbital ordering.

However, the orbital degrees of freedom are not completely quenched by the crystal distortion and there is a sub-

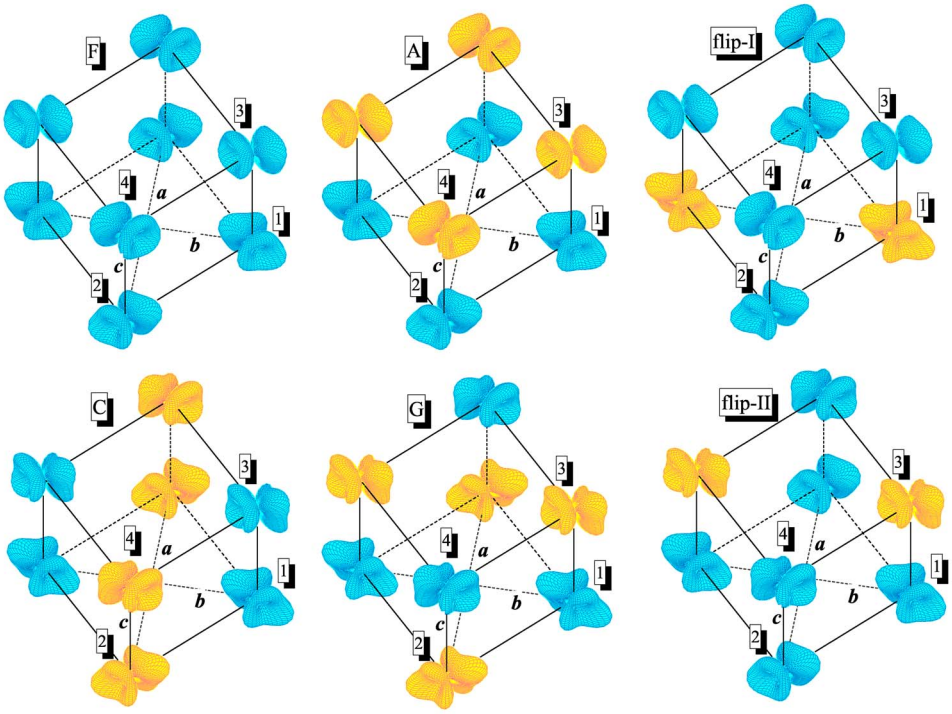

FIG. 12. (Color online) Distribution of the charge density around V sites in various magnetic phases of monoclinically distorted YVO_3, as obtained in the Hartree-Fock calculations. Different magnetic sublattices are shown by dark gray (blue) and light gray (yellow) colors.

stantial variation of the orbital structures depending on the magnetic state, which can be seen already in the distribution of the charge density shown in Fig. 12. Nevertheless, the basic shape of the G-type AFM orbital ordering pattern is clearly seen in all magnetic structures. This appears to be sufficient to stabilize the experimentally observed C-type AFM phase, which emerges as the ground state already at the level of HF calculations (Table IV). The correlation effects play a very important role. They additionally stabilize the C-type AFM ground state and reverse the order of other magnetic states (e.g., F and A in Table IV).

The orbital ordering in the plane (3,4) clearly reminiscent of the one observed in the orthorhombic phase (Fig. 10). The shape of the orbitals in the plane (1,2) appears to be more distorted.

The behavior of interatomic magnetic interactions in the high-temperature phase of YVO_3 deserves a particular attention. The experimental spin-wave spectrum shows a clear splitting into acoustic and optical branches, which are separated by a 5 meV gap in the middle, $\mathbf{q}_m=(0,0,\pi/2c)$, point of the first Brillouin zone along the [001] direction.[16] Originally, the splitting was thought to be due to the dimerization effects associated with a orbital Peierls state, which causes the alternation of the strong and weak ferromagnetic bonds along the **c** direction.[16] However, such a dimerization seemsto conflict with the C_{2h}^5 symmetry of the monoclinic phase (nevertheless, see also the footnote in Ref. 35). More recently, the puzzling splitting of the experimental magnon spectrum has been explained by the difference of interatomic magnetic interactions in the adjacent **ab** planes, which is expected for the C_{2h}^5 symmetry.[29] This effect is clearly seen in our HF calculations: while the AFM exchange coupling in the plane (3,4) does not change so much in comparison with the orthorhombic phase, the one in the plane (1,2) drops by almost 4 meV (referring to the C-type AFM state in Table IV). The value of the gap in the point $\mathbf{q}_m$ can be estimated in the linear spin-wave theory as

$$\Delta_{SW} = 2J_{13}|\sqrt{1-4J_{12}/J_{13}} - \sqrt{1-4J_{34}/J_{13}}|.$$

Then, using results of HF calculations we obtain $\Delta_{SW} \approx 6.2$ meV, which is in fair agreement with the experimental finding. We can further speculate that the ferromagnetic coupling J_{13} is overestimated in the HF approximation due to the lack of the correlations effects (in the next section we shall see that this is indeed the case for the totally ferromagnetic $YTiO_3$). Therefore, the correlation effects may also reduce Δ_{SW}, which is proportional to J_{13}.

TABLE IV. Magnetic interactions ($J_{\mathbf{RR}'}$), Hartree-Fock energies (E_{HF}), and total energies (E_{tot}) in the monoclinic phase of YVO_3 (77 K$<T<$116 K). The energies are measured from the most stable magnetic state in meV per one formula unit. The magnetic interactions are measured in meV. The total energy is defined as Hartree-Fock energy plus correlation energies (E_C) in the second order of perturbation theory, $E_{tot}=E_{HF}+E_C$.

Phase	J_{12}	J_{13}	J_{24}	J_{34}	E_{HF}	E_{tot}
F	0.1	2.7	2.7	−3.5	11.7	17.5
A	−0.3	2.5	2.5	−3.4	14.0	17.1
C	−0.9	2.2	2.2	−4.5	0	0
G	−1.6	1.8	1.8	−4.8	6.6	7.2
Flip I	−1.8	1.6	2.5	−3.4	11.5	14.2
Flip II	−0.4	2.3	2.8	−4.8	4.4	6.5

B. $YTiO_3$

$YTiO_3$ is a d^1 compound. The lattice distortion splits off one t_{2g} level to the low-energy part of the spectrum (Fig. 8),

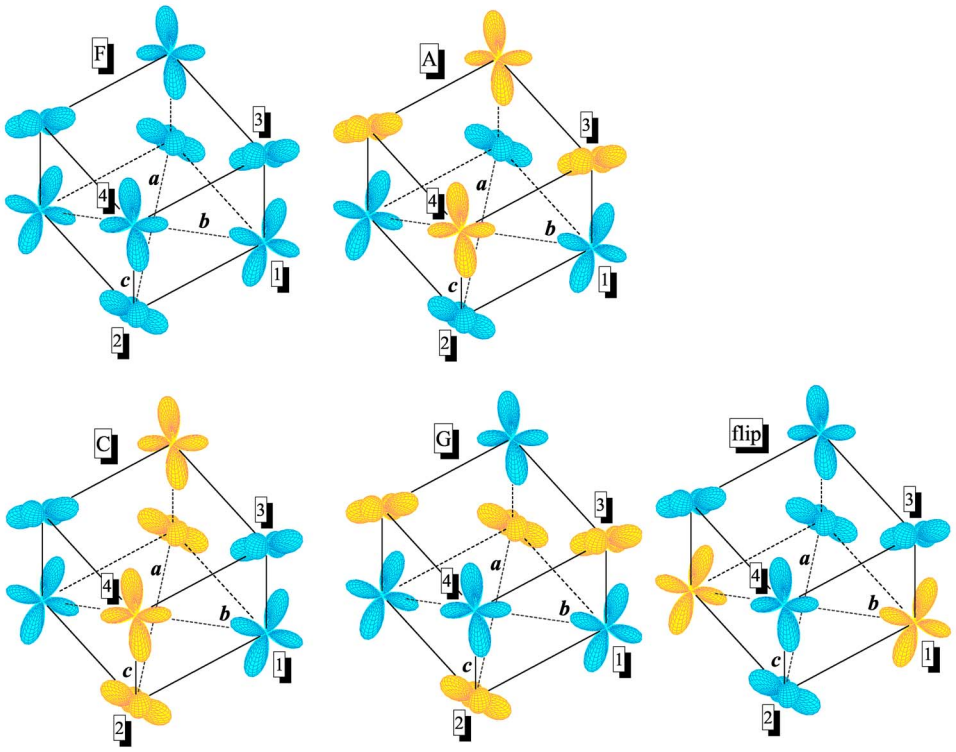

FIG. 13. (Color online) Distribution of the charge density around Ti sites in various magnetic phases of $YTiO_3$, as obtained in the Hartree-Fock calculations. Different magnetic sublattices are shown by dark gray (blue) and light gray (yellow) colors.

which is just enough for trapping one d electron at each Ti site. Therefore, the situation is similar to YVO_3. The lowest t_{2g} level is separated from the middle one by a 109 meV gap, which is comparable with the magnitude of the CF splitting in YVO_3.

The lattice distortion stabilizes the orbital ordering pattern, which is shown in Fig. 13. In this case, the orbital degrees of freedom are strongly quenched by the crystal distortion, and not only the charge densities but also the interatomic magnetic interactions, which are more sensitive to the change of the orbital ordering, only weakly depend on the magnetic state (Table V). Partly, this is because of the large value of the on-site Coulomb interaction $\mathcal{U}$ obtained in $YTiO_3$ in comparison with other perovskite oxides (Table II). Therefore, the superexchange contribution to the orbital ordering is expected to be smaller in $YTiO_3$, and the CF splitting will clearly dominate. The obtained orbital ordering pattern is in an excellent agreement with the results of LDA $+U$ calculations by Sawada and Terakura,[27] and the experimental measurements using the nuclear magnetic resonance (Ref. 7), the polarized neutron diffraction (Ref. 8), and the soft x-ray linear dichroism (Ref. 10).

The observed orbital ordering patter is compatible with the ferromagnetic ground state, which easily emerges at the level of HF calculations.[19,27] The same trend is clearly seen in our HF studies, where both the order $F \rightarrow A \rightarrow C \rightarrow$ flip $\rightarrow G$ and the total energy differences between different magnetic states are well consistent with the results of LDA$+U$ calculations by Sawada and Terakura.[27]

The correlation effects are important. Similar to YVO_3, they tend to additionally stabilize the AFM configurations and destabilize the ferromagnetic ground state. The situation is very fragile, and after taking into account the correlation effects, the energy difference between the F state and the next A-type AFM state becomes only 0.1–0.8 meV per one formula unit. In fact, for the titanites, we can apply two independent schemes for studying the correlation effects: one is the second order perturbation theory and the other one is

TABLE V. Magnetic interactions ($J_{\mathbf{RR}'}$), Hartree-Fock energies (E_{HF}), total energies (E_{tot}), and superexchange energies (E_{SE}) in $YTiO_3$. The energies are measured from the most stable magnetic state in meV per one formula unit. The magnetic interactions are measured in meV. The total energy is defined as Hartree-Fock energy plus correlation energies (E_C) in the second order of perturbation theory, $E_{\mathrm{tot}}=E_{\mathrm{HF}}+E_C$. E_{SE} is defined as the total energy in the superexchange approximation.

Phase	J_{12}	J_{13}	J_{24}	J_{34}	E_{HF}	E_{tot}	E_{SE}
F	3.9	1.2	1.2	3.9	0	0	0
A	3.9	1.1	1.1	3.9	2.0	0.8	0.1
C	3.2	1.1	1.1	3.2	14.4	10.9	12.1
G	3.2	1.0	1.0	3.2	16.2	12.5	13.9
Flip	3.2	1.1	1.1	3.9	8.2	6.1	6.7

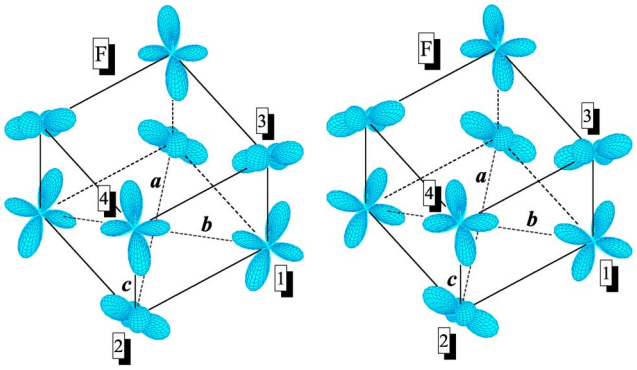

FIG. 14. (Color online) Orbital ordering in the ferromagnetic phase of $YTiO_3$ computed with (left) and without (right) crystal-field splitting.

the theory of superexchange interactions, taking into account the multiplet structure of the excited states. For $YTiO_3$, both schemes provide a very consistent picture, apart from the small quantitative differences, which are always inevitable for two very different approximations.

Yet, the magnetic behavior of $YTiO_3$ poses several open questions, which are not fully understood.

First of all, $YTiO_3$ is an exceptional example amongst t_{2g} perovskite oxides, where the ferromagnetic ground state is anticipated on the basis of canonical Goodenough-Kanamori-Anderson rules for the superexchange interactions in the simple cubic structure. This immediately revives the idea of Kugel and Khomskii about the superexchange-driven orbital ordering and the concomitant Jahn-Teller distortion, which was intensively discussed in the context of $KCuF_3$.[54] Then, it is reasonable to ask whether the experimental orbital ordering in $YTiO_3$ can be stabilized by the pure superexchange mechanism, without the CF splitting. This can be easily checked by substituting $h^{\alpha\beta}_{\mathbf{RR}}=0$ into the kinetic-energy part of our model Hamiltonian. The results of these calculations are shown in Fig. 14. Surprisingly, the orbital ordering *in the ferromagnetic state* is practically the same with and without the CF splitting. The interatomic magnetic interactions, $J_{12}=4.3$ meV and $J_{13}=1.6$ meV, are also consistent with the data listed in Table V, and which include the effect of the CF splitting. This naturally explains results of our previous work (Ref. 28), where similar orbital ordering and interatomic magnetic interactions have been obtained by taking into account only the covalent part of the CF splitting and neglecting the nonsphericity of the Madelung potential. Therefore, it is tempting to conclude that the orbital ordering in $YTiO_3$ is driven by the superexchange interactions, and the lattice distortion simply follows the anisotropic distribution of the charge density associated with this orbital state. However, the situation is not so simple, because our calculations have been performed using the crystal structure corresponding to the room temperature,[6] which is considerably higher than the Curie temperature ($T_C \approx 30$ K, Ref. 8). Furthermore, the particular orbital ordering shown in Fig. 14 in the absence of the CF splitting takes place only in the ferromagnetic phase. For example, had we changed the magnetic state, our orbital ordering pattern would have been also different. Therefore, it seems that a more plausible scenario for $YTiO_3$ is that the lattice distortion goes first and sets up the experimental orbital ordering pattern and the ferromagnetic ground state. Nevertheless, the good agreement between two orbital states shown in Fig. 14 is really curious. Is it a simple coincidence or is there some physical meaning behind this result? We would like to emphasize again that the situation is totally different from YVO_3 considered in Sec. V A.

Another group of questions is related with the behavior of interatomic magnetic interactions. The first puzzling feature is the nearly isotropic experimental spin-wave spectrum reported by Ulrich *et al.*,[9] which cannot be explained in terms of interatomic magnetic interactions derived from the first-principles electronic structure calculations. For example, the parameters listed in Table V are clearly anisotropic, where the interatomic magnetic interactions along the **c** axis are much weaker than those in the **ab** plane. A similar conclusion is expected from the analysis of the total energy differences reported by Sawada and Terakura.[27] Since this anisotropy of magnetic interactions is directly related with the particular form of the orbital ordering, it seems that the inelastic neutron-scattering data by Ulrich *et al.* are in an apparent disagreement not only with the results of first-principles electronic structure calculations but also with a number of other experimental data, which report the same type of the orbital ordering.[7,8,10] Clearly, this controversy deserves further analysis, apparently on the both theoretical and experimental sides.

The behavior of interatomic magnetic interactions predetermines not only the form of the magnon spectrum, but also the absolute value of T_C. If the magnetic properties of $YTiO_3$ are indeed controlled by the large lattice distortion, which is set up far above T_C, it should be a good Heisenberg ferromagnet. This is directly seen in our HF calculations for $YTiO_3$, where the interatomic magnetic interactions are the least sensitive to the magnetic state (Table V). Then, the applicability of the Heisenberg model is no longer restricted by infinitesimal rotations of the spin magnetic moments, and T_C can be easily evaluated using the standard expressions, which are well known in the theory of Heisenberg magnets.[59] The simplest one is the mean-field formula, $3k_BT_C^{\mathrm{MF}}=4J_{12}+2J_{13}$, where the prefactor $S(S+1)$ is already included in the definition of our exchange parameters, though with some approximations for the spin-1/2.[60] By combining this expression with the HF approximation for the exchange interactions, one finds $T_C^{\mathrm{MF}}=64$ K, which exceeds the experimental value by a factor of 2. However, T_C^{MF} does not include spontaneous fluctuations and correlations between the motion of the neighboring spins. This is exactly the point where the anisotropy of exchange interactions can help to reduce the theoretical value of T_C. Indeed, according to the Mermin-Wagner theorem,[61] the two-dimensional Heisenberg model does not support any long-range spin order at any nonzero temperature. Therefore, since for $J_{13}/J_{12} \ll 1$ the system will eventually approach this two-dimensional limit, it is reasonable to expect a substantial reduction of T_C. In order to describe these effects quantitatively, one can use the spherical approximation for the Heisenberg model,[59] where $3k_BT_C=1/[\Sigma_{\mathbf{k}}(J_0-J_{\mathbf{k}})^{-1}]$, $J_{\mathbf{k}}=\Sigma_{\mathbf{R}'}J_{\mathbf{RR}'}e^{i\mathbf{k}\cdot\mathbf{R}'}$, and the summation over $\mathbf{k}$ is restricted by the first Brillouin zone. Then, using

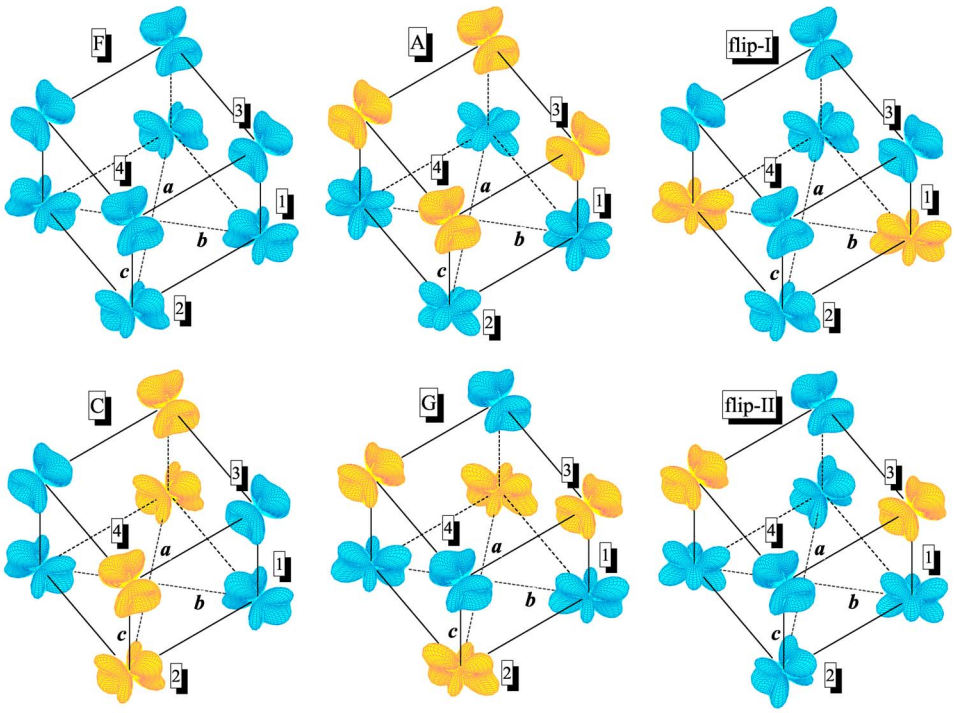

FIG. 15. (Color online) Distribution of the charge density around V sites in various magnetic phases of $LaVO_3$, as obtained in the Hartree-Fock calculations. Different magnetic sublattices are shown by dark gray (blue) and light gray (yellow) colors.

parameters extracted from the HF calculations, one finds T_C=36 K, which can be further reduced by correlation effects. For example, by mapping the total energy change obtained in the second order of perturbation theory and in the theory of superexchange interactions onto the Heisenberg model, we obtain T_C=27 and 28 K, respectively, which is in fair agreement with the experimental data.

C. $LaVO_3$

The monoclinic $LaVO_3$ has two inequivalent V sites. Contrary to YVO_3, these sites differ not only by the direction, but also by the magnitude of the CF splitting (Table VIII), which can be estimated as 78 and 152 meV for the sites 1 and 3, respectively (referring to the splitting between middle and highest t_{2g} levels). Therefore, already from this very simple analysis of the CF splitting one can expect very different behavior of the orbital degrees of freedom in different **ab** planes: the strong quenching in the plane (3,4), and a relative flexibility in the plane (1,2) (Fig. 2). Thus, the situation is qualitatively different from YVO_3.

Furthermore, the effective Coulomb interaction $\mathcal{U}$ is *smaller* in $LaVO_3$ (Table II), while the transfer integrals between nearest neighbors are generally larger (Fig. 6). Therefore, the energy gain caused by the virtual hoppings of an electron to the neighboring sites (and back), which lead to the superexchange coupling (see Sec. IV C), will be generally larger in $LaVO_3$. This energy gain can be further minimized by adjusting the form of the spin and orbital ordering. The latter effect is known as the Kugel-Khomskii mechanism of the spin and orbital ordering, which is a generalization of Goodenough-Kanamori-Anderson rules.[54] The Kugel-Khomskii mechanism will certainly play a more important role in $LaVO_3$ (in comparison with YVO_3), and, as we will see in a moment, can even compete with the CF splitting.

These trends are clearly seen in our HF calculations (Fig. 15): the orbital ordering in the plane (1,2) strongly depend on the magnetic state and one can clearly distinguish (at least) two types of the orbital-ordering pattern realized, on the one hand, in the phases *F* and *C*, and, on the other hand, in the phases *A* and *G*. In fact, even such a division is only qualitative, because there is still a substantial difference between orbital states realized, for example, in the phases *A* and *G*, which will be seen in the behavior of interatomic magnetic interactions. Therefore, it is perhaps right to say that in $LaVO_3$, the experimental orbital ordering is partly concomitant to the magnetic ordering via the Kugel-Khomskii mechanism.[54] This seems to agree with the experimental data, which show that in La-based compounds, the orbital ordering develops only few degrees below the magnetic Néel temperature (T_N).[62] This is again different from YVO_3, for

TABLE VI. Magnetic interactions ($J_{\mathbf{RR}'}$), Hartree-Fock energies (E_{HF}), and total energies (E_{tot}) in $LaVO_3$. The energies are measured from the most stable magnetic state in meV per one formula unit. The magnetic interactions are measured in meV. The total energy is defined as Hartree-Fock energy plus correlation energies (E_C) in the second order of perturbation theory, $E_{\mathrm{tot}}=E_{\mathrm{HF}}+E_C$.

Phase	J_{12}	J_{13}	J_{24}	J_{34}	E_{HF}	E_{tot}
F	−5.1	6.6	6.6	−1.7	21.0	30.8
A	3.8	2.1	−4.5	−2.4	20.6	24.1
C	−4.8	6.0	6.0	−1.8	0	0
G	−6.3	−4.4	−4.4	−2.4	7.6	11.1
Flip I	7.7	0.6	5.8	−1.7	9.8	15.0
Flip II	−6.2	−4.0	5.8	−3.1	12.7	16.9

which the orbital-ordering temperature is substantially higher than T_N.

The change of the orbital ordering is reflected in the behavior of interatomic magnetic interactions, which not only depend on the magnetic states, but can even change the signs (Table VI). In such a situation, the total energy may have several local minima, realized for those magnetic states where the signs of interatomic magnetic interactions are consistent with the type of the imposed spin ordering. We have found at least two such minima, corresponding to the *C*-type AFM ground state and the *G*-type AFM state, which has higher energy. Another interesting situation is realized in the *A* phase, where the orbitals in the (1,2) plane are able to rearrange so to form the ferromagnetic spin coupling in the bond 1-2 and the AFM spin coupling in the bond 2-4, which are consistent with the *A*-type AFM spin structure. However, the orbital ordering in the plane (3,4) is frozen by the CF splitting. Therefore, the spin coupling in the bond 1-3 remains antiferromagnetic and the spin coupling in the bond 1-3 becomes ferromagnetic, which make the whole *A*-type AFM spin structure unstable. Thus, we do not quite agree with the conclusions about the complete quenching of the orbital ordering in these distorted perovskite compounds.[29] This is not generally true and $LaVO_3$ is clearly an exception.

Thus, on the basis of our calculations we can propose the following model for the spin and orbital ordering in $LaVO_3$:

(i) In every second monoclinic **ab** plane (we will call them "quenched planes"), the orbital degrees of freedom are quenched by the crystal distortion, which leads to the robust orbital ordering and develops the AFM coupling between spin magnetic moments within these planes.

(ii) In the adjacent planes, the crystal distortion is relatively small, so that the orbitals are rather flexible and can follow the spin ordering via the Kugel-Khomskii mechanism.

(iii) Then, there are only three magnetic structures, which are compatible with the translation symmetry of the monoclinic phase and the AFM spin coupling in the quenched **ab** planes. These are *C*, *G*, as well as (strongly frustrated) flip-II structure.

(iv) If the intra-atomic exchange (Hund's rule) coupling $\mathcal{J}$ is finite, the ferromagnetic spin coupling between the planes can be easily stabilized by AFM orbital correlations, as it was suggested by model (mean-field and exact diagonalization) calculations for cubic vanadates in the realistic parameters range $\eta=\mathcal{J}/\mathcal{U}\sim 0.2$ (see Table II).[21] This naturally explains the origin of the *C*-type AFM ground state in $LaVO_3$.

In our scenario, the relative flexibility of the orbital degrees of freedom in one of the **ab** planes plays an important role and naturally explains the fact that the spin and orbital ordering in $LaVO_3$ develop almost simultaneously with the decrease of the temperature.[62] Note however, that the quenching of the orbital degrees of freedom in another **ab** plane poses a severe constraint on the possible form of orbital and spin magnetic structures in $LaVO_3$. For example, similar to YVO_3, one can probably safely rule out the appearance of the orbital dimerization also in $LaVO_3$, which is only possible between degenerate t_{2g} orbitals in the adjacent **ab** planes. Also, as we will see in Sec. V E, the orbital magnetic moments are strongly quenched by the crystal distortion, even in $LaVO_3$.

Since the interatomic magnetic interactions depend on the magnetic state, the simple Heisenberg model may be used only for the analysis of local perturbations around each magnetic state. Then, it is reasonable to expect a gap $\Delta_{SW} \approx 6.8$ meV between acoustic and optical branches of the spin-wave spectrum, similar to the one observed in the *C*-type AFM phase of YVO_3.[16] However, the Heisenberg model is no longer valid for the analysis of the transition temperature (unlike in $YTiO_3$), which should take into account a possible change of the orbital states in the course of thermodynamic average.

Similar to YVO_3 and $YTiO_3$, the correlation effects play a very important role also in $LaVO_3$ and additionally stabilize the *C*-type AFM ground state.

D. $LaTiO_3$

$LaTiO_3$ is a puzzling system. It has the smallest CF splitting among the distorted perovskite oxides (about 37 meV between lowest and middle t_{2g} levels, Fig. 8), which formally leaves a room for the orbital fluctuations. On the other hand, the possible variations of the orbital structure appear to be bounded by certain constraint conditions. For example, although the orbital ordering depends on the magnetic state, this dependence is not particularly strong, as it is clearly seen from the HF calculations, where the basic shape of the orbital-ordering pattern remains the same for different magnetic states (Fig. 16). There is certainly some variation of the orbital ordering, which can be seen already on the plot. However, this variation does not seem to change the qualitative conclusion about the form of interatomic magnetic interactions and the magnetic ground state of $LaTiO_3$.

Unfortunately, this conclusion is not consistent with the experimental data. In this sense, there is a clear difference of $LaTiO_3$ from other perovskite compounds considered in this work, despite the fact that we have used absolutely the same procedure for construction and solution of the model Hamiltonian.

The magnetic ground state is expected to be of the *A* type, as it is clearly seen from the total-energy calculations as well

TABLE VII. Magnetic interactions ($J_{\mathbf{RR}'}$), Hartree-Fock energies (E_{HF}), total energies (E_{tot}), and superexchange energies (E_{SE}) in $LaTiO_3$. The energies are measured from the most stable magnetic state in meV per one formula unit. The magnetic interactions are measured in meV. The total energy is defined as Hartree-Fock energy plus correlation energies (E_C) in the second order of perturbation theory, $E_{tot}=E_{HF}+E_C$. E_{SE} is defined as the total energy in the superexchange approximation.

Phase	J_{12}	J_{13}	J_{24}	J_{34}	E_{HF}	E_{tot}	E_{SE}
F	4.5	−1.2	−1.2	4.5	5.0	17.7	1.6
A	3.6	−3.3	−3.3	3.6	0	0	0
C	1.0	−2.0	−2.0	3.4	19.6	26.3	14.2
G	2.0	−4.9	−4.9	2.0	11.5	11.0	9.0
Flip	1.3	−4.5	−0.4	4.6	7.7	11.4	5.7

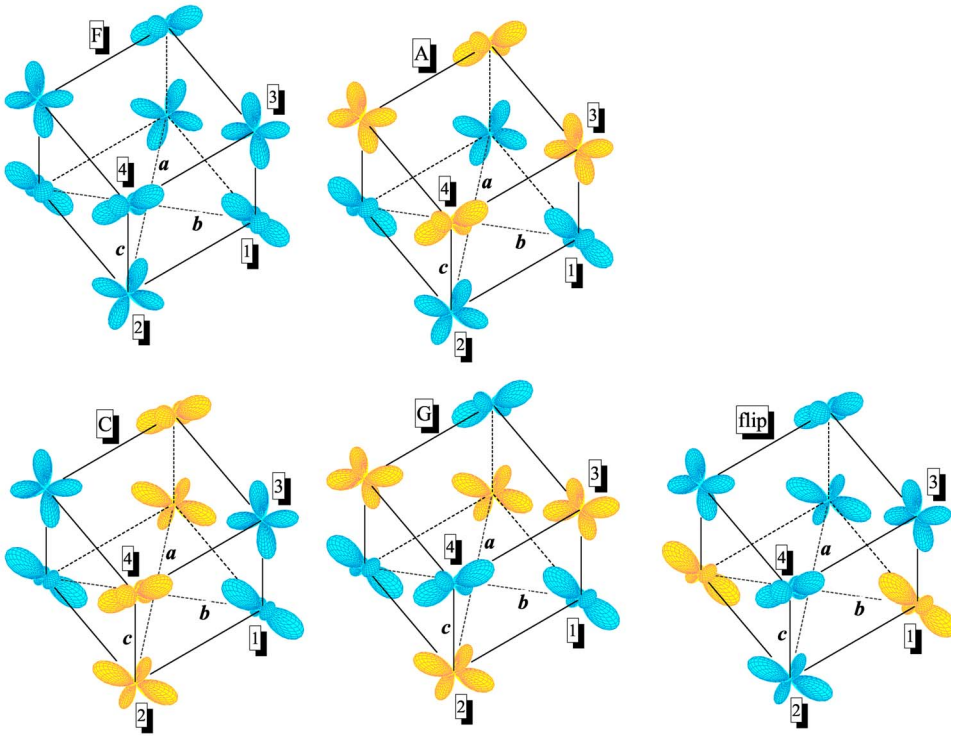

FIG. 16. (Color online) Distribution of the charge density around Ti sites in various magnetic phases of $LaTiO_3$, as obtained in the Hartree-Fock calculations. Different magnetic sublattices are shown by dark gray (blue) and light gray (yellow) colors.

as from the behavior of interatomic magnetic interactions (Table VII), although experimentally, it is totally antiferromagnetic G type.[11] The magnetic interactions are sensitive to the magnetic ordering. However, other magnetic states appear to be unstable and the form of interatomic magnetic interactions in each magnetic state systematically leads to the A-type antiferromagnetism. This conclusion is totally consistent with our previous work,[28] where we did not consider the nonsphericity of the Madelung potential and the contribution of this nonsphericity to the CF splitting.

Then, what is missing in our calculations, or maybe even more generally, in our understanding of the magnetic properties of $LaTiO_3$? Below we discuss several plausible scenarios.

(i) One possibility is that the effect of the crystal distortion maybe still underestimated. Particularly, we tried to follow the idea of Refs. 23 and 24, and additionally scaled the contribution of the Madelung term to the CF splitting by multiplying the right-hand side of Eq. (2) by a constant. This corresponds to the change of the dielectric constant, which in Refs. 23 and 24 was treated as an adjustable parameter. We have found that in order to obtain the experimentally observed G-type antiferromagnetic ground state, the dielectric constant should be reduced by a factor of 4 (Fig. 17). Then, the exchange interactions become nearly isotropic ($J_{12}=-3.3$ and $J_{13}=-3.5$ meV) and only weakly depend on the magnetic state. Hence, $LaTiO_3$ is expected to be a good Heisenberg antiferromagnet, in agreement with experimental inelastic neutron-scattering data. The latter reveal nearly isotropic spin-wave dispersion, which can be fitted in terms of a single exchange interaction parameter $J=J_{12}=J_{13}=-15.5S^2 \approx -3.9$ meV.[11] The same parameter J can explain the experimental value of the Néel temperature $T_N \approx 150$ K.[11] Thus, we totally agree with the authors of Refs. 23 and 24 that the Madelung term alone could explain several experimental features of $LaTiO_3$. The only problem is that, according to the electronic structure calculations, this effect is too small. One can of course try to blame LDA for this failure. However, why does this problem occur only for $LaTiO_3$ while for other perovskite compounds our method works reasonably well? We believe that if the story about the structural origin of the G-type antiferromagnetism in $LaTiO_3$ does make sense, it is more likely that the real magnitude of the crystal distortion in $LaTiO_3$ is still undisclosed experimentally. This seems to be reasonable, because the structural data for the distorted perovskite oxides are still in the process of steady refinement.[12,14,15]

(ii) Other scenarios are related with correlation effects, which are not taken into account by the HF calculations. There is no doubt that they must play an important role also in $LaTiO_3$. However, it seems that there is no straightforward

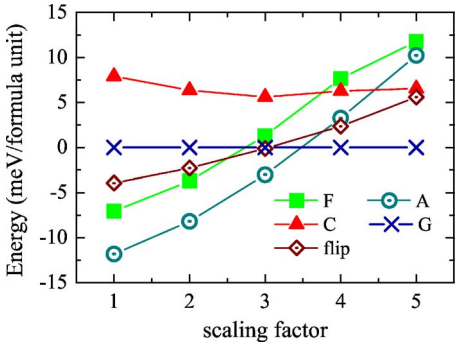

FIG. 17. (Color online) Total energies measured relative to the G-type antiferromagnetic state as obtained in the Hartree-Fock calculations after scaling the Madelung contribution to the crystal-field splitting.

scheme which would allow us to incorporate these effects easily into the electronic structure calculations. The second-order perturbation theory and the theory of superexchange interactions, which we tried, are definitely not enough. They do substantially change the total energies of the HF method. However, the conclusions strongly depend on the approximation which we use (Table VII). For example, from the second order perturbation theory, it seems to be clear that the correlation effects tend to stabilize the *G*-type AFM state: the correlations change the order of the magnetic states and somewhat lower the energy of the *G*-type AFM state relative to the *A* state. However, this is not enough to make the *G*-type AFM state to be the ground state of $LaTiO_3$.[63] The latter trend is also seen for the superexchange approach. However, the superexchange method tends to lower also the energies of other magnetic states (relatively to the *A*-type AFM state), apparently through the small change of the orbital ordering. This is in straight contrast with the more distorted $YTiO_3$, where two different methods provide a consistent picture for the role played by the correlation effects (Table V).

(iii) The theory of the orbital liquid is just an opposite case to the theory of CF splitting as these two effects are incompatible with each other. Although the formation of the orbital liquid in the cubic t_{2g} lattice is a many-electron effect, the necessary prerequisite, which should exist already at the mean-field level, is an infinite degeneracy of the magnetic ground state.[20] In this sense, we were very surprised by the fact that, although our CF splitting for $LaTiO_3$ is small, which is sometimes regarded as the strong support for the orbital liquid theory, we do not observe such a degeneracy in the Hartree-Fock method: all HF calculations steadily converge to a single solution for the orbital-ordering pattern, which is shown in Fig. 16, irrespectively on the starting conditions and the size of the supercell. Thus, we believe that it is still an open (and very interesting) question whether the orbital liquid will be realized as the ground state of $LaTiO_3$ or not. One clue may be the absolute value of the correlation energy in $LaTiO_3$, which appears to be larger than in other perovskite oxides. For example, the second order perturbation theory yields E_C=−11 and −19 meV per one formula unit, correspondingly for the ferromagnetic and *G*-type AFM phase of $LaTiO_3$. These values are already comparable with the magnitude of the CF splitting in $LaTiO_3$. Therefore, it is possible that the correlation effects should be considered *at the first place*, and the simple HF theory for the spin and orbital ordering with the subsequent inclusion of the correlation effects as a perturbation to the HF ground state may not be appropriate here. We do not rule out such a possibility. In such a situation, it is perhaps more practical to get rid of the perturbation-theory expansion near the nondegenerate HF ground state, which was pursued in this work, and derive an approximate ground state from the diagonalization of a many-electron Hamiltonian matrix constructed in the basis of some limited number of specially selected Slater determinants, as it is done, for example, in the path-integral renormalization group method.[5,64]

Thus, one of the challenging problems in the theory of distorted perovskite oxides remains to be the explanation of the *G*-type AFM ground state in $LaTiO_3$. Definitely, we need a more rigorous theory for the correlation effects. But, will it be enough, or do we need a more radical refinement of our starting model, given by Eq. (1), in the case of $LaTiO_3$?

E. Spin-orbit interaction and magnetic ground state

The spin-orbit interaction in the distorted perovskite oxides will generally lead to the noncollinear spin alignment, which obeys certain symmetry rules.[65] The spin magnetic moments, aligned along one of the orthorhombic axes, will be subjected to certain rotational forces, coming both from the Dzyaloshinsky-Moriya interactions and from the minimization of single-ion anisotropy energies,[66,67] which lead to the spin canting and the appearance of nonvanishing components of the spin-magnetization density along two other directions. The type of the magnetic ordering for all three projection of the spin-magnetization density is generally different. Thus, each magnetic structure can be generally abbreviated as *X*-*Y*-*Z*, where *X*, *Y*, and *Z* is the type of the magnetic ordering (*F*, *A*, *C*, or *G*) formed by the projections of the spin magnetic moments onto the orthorhombic axes **a**, **b**, and **c**, respectively.[68] The orbital magnetic structure has the same symmetry, although it may have a different origin of the canting, which arises mainly from the minimization of the single-ion anisotropy energy at individual transition-metal sites. Generally, the spin and orbital magnetic moments are not collinear to each other.[69]

Results of HF calculations, which take into account the spin-orbit interaction, are summarized in Table VIII. The magnetic ground state of $YTiO_3$ is *G*-*A*-*F*, in agreement with the neutron scattering data.[9] The ferromagnetic moment is aligned along the **c** axis, and the canting angle is relatively small. The absolute values of the spin and orbital magnetic moments are different from those reported in our previous work.[28] The difference is related with the additional transformation to the LMTO basis, employed in the present work, which allows us to decompose the magnetization densities over different atomic sites and evaluate the local spin and orbital magnetic moments directly at the transition-metal sites, whereas in Ref. 28 these moments have been calculated in the Wannier basis, which had a substantial weight at other (e.g., oxygen) sites. This comparison clearly shows that the covalent effects play a very important role and allow us to explain the substantial reduction of the local magnetic moments at the transition-metal sites. As it was already discussed in Sec. V B, the correlation effects in $YTiO_3$ favor the AFM coupling and systematically lower the energies of all AFM states relative to the ferromagnetic ground state (see Table V). Then, it is reasonable to expect that after including the spin-orbit interaction, the correlation effects will lead to an additional spin canting away from the collinear ferromagnetic state. Such an effect is clearly seen in our calculations. For example, in the framework of superexchange approach we have obtained the following values of spin and orbital magnetic moments (in μ_B, referred to as site 1): $\boldsymbol{\mu}_S$ =(−0.02,−0.29,0.77) and $\boldsymbol{\mu}_L$=(−0.05,0.02,−0.03). It readily explains the experimental values reported for the *F* and *G* components of the magnetic moments, correspondingly along the **c** and **a** axes,[9] while the *A*-type AFM com-

TABLE VIII. The type of the magnetic ground state, the vectors of spin ($\boldsymbol{\mu}_S$) and orbital ($\boldsymbol{\mu}_L$) magnetic moments (in μ_B) at given transition-metal sites, and the values of the band gap (E_g, in eV) as obtained in Hartree-Fock calculations. For the magnetic ground state, three capital letters denote the type of the magnetic ordering for three projections of the magnetic moments onto the orthorhombic axes **a**, **b**, and **c**, respectively. For the spin and orbital magnetic moments at the given transition-metal sites, these three projections are specified by the vectors $\boldsymbol{\mu}_S$ and $\boldsymbol{\mu}_L$, respectively. The positions of the transition-metal sites are shown in Fig. 2.

Compound	Phase	Ground state	Site	$\boldsymbol{\mu}_S$			$\boldsymbol{\mu}_L$			E_g
$YTiO_3$	*o*	*G-A-F*	1	(−0.00,	−0.09,	0.84)	(−0.05,	0.01,	−0.03)	1.1
$LaTiO_3$	*o*	*C-F-A*	1	(0.02,	−0.17,	0.76)	(0.10,	0.03,	−0.08)	0.6
YVO_3	*o*	*F-C-G*	1	(−0.02,	0.00,	1.65)	(0.00,	−0.00,	−0.17)	1.2
YVO_3	*m*	*C-A-C*	1	(−0.74,	0.08,	1.48)	(0.07,	−0.04,	−0.16)	1.0
			3	(−0.78,	−0.03,	1.48)	(0.05,	0.04,	−0.07)	
$LaVO_3$	*m*	*A-C-A*	1	(−0.05,	1.64,	−0.05)	(0.09,	−0.18,	0.11)	0.9
			3	(0.06,	1.63,	0.05)	(−0.05,	−0.09,	−0.06)	

ponent along the **b** axis is somewhat larger in our calculations. The reason is not clear. The orbital magnetic moments in $YTiO_3$ are strongly quenched by the crystal field.

The orthorhombic YVO_3 has nearly collinear magnetic structure, where the *G*-type AFM moment is aligned along the **c** axis. The total magnetic moment $(\boldsymbol{\mu}_S+\boldsymbol{\mu}_L)\|\mathbf{c}=1.48\mu_B$, parallel to the **c** axis, is in the excellent agreement with the experimental value of $1.45\mu_B$ reported by Blake *et al.* and corresponding to $T=65$ K.[14] Ulrich *et al.* reported somewhat larger value of $1.72\mu_B$, also oriented along **c**.[16] The weak ferromagnetic component along the **a** direction has been also observed experimentally.[13] Details of the magnetic ordering in the monoclinic phase of YVO_3 are somewhat controversial. Blake *et al.* reported the *C*-type AFM ordering for both **b** and **c** components of the magnetic moments in the orthorhombic *Pbnm* notations, which correspond to the **a** and **c** directions in the monoclinic $P2_1/a$ notations.[14] This is totally consistent with our finding. The quantitative difference can be explained by the finite temperature effects in the intermediate phase.[29] Furthermore, we predict the *A*-type *antiferrimagnetic* ordering for the remaining **b** component (in the $P2_1/a$ notations), which implies nearly antiferromagnetic alignment of the **b** projections of the magnetic moments in the adjacent **ab** planes. However, since the sites 1 and 3 are not fully equivalent in the monoclinic structure, the **b** projections do not compensate each other, and the system exposes a net magnetic moment parallel to **b**, which can couple to the magnetic field.[13] The *antiferrimagnetic* ordering obtained for the **b** component is also consistent with the temperature-induced magnetization reversal behavior of YVO_3 observed by Ren,[13] and could be a natural explanation for this effect. More generally, it is right to say that the magnetic coupling along the **c** direction of the monoclinic phase is always either ferrimagnetic or antiferrimagnetic, because the sites 1 and 3 are *not equivalent*.

The *C-A-C* magnetic ground state appears to be different from the magnetic structure reported by Ulrich *et al.*, who have observed the *C*-type AFM ordering for the **a** and **b** components, and the *G*-type AFM ordering for the remaining **c** component (apparently, in the *Pbnm* notations).[16] One possible explanation for this difference could be the coexistence of several magnetic structures in a narrow energy range. Such a behavior has been indeed observed in our HF calculations: in addition to the *C-A-C* state we were able to obtain another self-consistent solution corresponding to the *A-C-F* phase with a slightly higher energy (about 0.04 meV per one formula unit, which is of the order of the magnetocrystalline anisotropy energy). The new phase has the following magnetic moments (in μ_B, where the first and second lines corresponds to the sites 1 and 3, respectively):

$$\boldsymbol{\mu}_S^1=(-0.07,\ 1.65,\ 0.05),\ \boldsymbol{\mu}_L^1=(\ 0.05,-0.15,-0.02),$$

$$\boldsymbol{\mu}_S^3=(\ 0.07,\ 1.67,\ 0.03),\ \boldsymbol{\mu}_L^3=(-0.09,-0.07,-0.02).$$

Although the exact form of the magnetic state *A-C-F* is still different from the observation by Ulrich *et al.*,[16] we can speculate that they probably used a different experimental setup which yielded the realization of another magnetic phase, which was different from the finding by Blake *et al.* (Ref. 14) and Ren *et al.* (Ref. 13). At least, their *C*-type AFM component parallel to the **ab** plane is qualitatively consistent with the form of the *A-C-F* phase obtained in our HF conclusions, and to a certain extent the results of HF calculations can be further modified by the correlation effects. Note also that in the present work we used the experimental structure reported by Black *et al.*[14] Therefore, it is not surprising that generally we have a better agreement also with the magnetic data of Black *et al.* rather than with the ones reported by Ulrich *et al.* Unfortunately, the details of the experimental crystal structure obtained for YVO_3 by the second group became available only recently,[70] when the present work was nearly completed.

In the case of $LaVO_3$ we were able to find three stable magnetic solutions: *A-C-A*, *C-A-C*, and *C-F-G*. The first two are similar to the *A-C-F* and *C-A-C* states, emerging in the monoclinic YVO_3. The only difference is that the *A-C-A* state has lower energy and, therefore, is realized as the magnetic ground state of $LaVO_3$. Like in YVO_3, the *A*-type state corresponds to the *antiferrimagnetic* alignment. Therefore, $LaVO_3$ is expected to have the net magnetic moment in the

ac plane. The third (*C*-*F*-*G*) solution has nearly collinear spin structure:

$$\boldsymbol{\mu}_S^1 = (-0.01, -0.06, \ 1.60), \ \boldsymbol{\mu}_L^1 = (\ 0.01, \ 0.13, -0.34),$$

$$\boldsymbol{\mu}_S^3 = (-0.03, -0.02, -1.61), \ \boldsymbol{\mu}_L^3 = (\ 0.01, \ 0.04, \ 0.14).$$

It corresponds to the stable *G*-type AFM phase emerging without the spin-orbit interaction (see Table III). Nevertheless, the *A*-*C*-*A* state appears to be well separated from the *C*-*A*-*C* and *C*-*F*-*G* states, correspondingly by 0.19 and 6.50 meV per one formula unit.

The quenching of the orbital magnetic moments in two different sublattices of monoclinic YVO_3 and $LaVO_3$ nicely correlates with the values of the CF splitting (Fig. 8), where larger CF splitting at the site 3 results in smaller orbital magnetization.

It is probably meaningless to discuss the relativistic effects in $LaTiO_3$, where we could not reproduce the correct magnetic ground state. We could agree with the criticism risen by Haverkort *et al.* (Ref. 41) that our CF splitting alone does not explain details of their spin-resolved photoemission spectra (actually, our value of the parameter $\langle \mathbf{L} \cdot \mathbf{S} \rangle$, obtained in the HF calculations after the transformation to the LMTO basis and the radial integration over the Ti sphere is about −0.13, which exceeds the experimental value by a factor of 2). However, it does not make sense to present as an alternative the results of calculations yielding the same *A*-type AFM ground state,[32] which totally agrees with our finding and (unfortunately) disagrees with the experiment, even though these calculations yield somewhat larger values of the CF splitting. As it has been already discussed in Sec. III A, different values of the CF splitting obtained by different authors are most likely related with the nonunique choice of the Wannier functions for the t_{2g} bands of the distorted perovskite oxides. One can formally adjust the theoretical CF splitting in order to meet certain demands of some particular class of the experimental data. However, will it solve a more fundamental problem related with the magnetic ground state of $LaTiO_3$?

In addition, we show in Table VIII the values of the band gap obtained in the HF calculations for the magnetic ground state. For $YTiO_3$, YVO_3, and $LaVO_3$ there is a good agreement with the experimental optical data.[15,71] However, for $LaTiO_3$ the experimental gap is substantially smaller (~0.1 eV).[71] This may indicate again the particular importance of correlation effects in $LaTiO_3$.

VI. SUMMARY AND CONCLUDING REMARKS

The main purpose of this work was to make a bridge between first-principles electronic structure calculations and model approaches for the strongly correlated systems, and illustrate how it works for the series of distorted t_{2g} perovskite oxides. The whole plan included three major steps: *first-principles electronic structure calculations*→*construction of the model Hamiltonian* for the isolated t_{2g} bands located near the Fermi level→*solution of this model Hamiltonian* using several different techniques. The choice of the distorted t_{2g} perovskite oxides was motivated by the fact that they represent a good example of the systems for which it is practically impossible to construct a relevant model Hamiltonian without the impact from the first-principles calculations: simply, the lattice distortion is too complex and there are too many model parameters, which cannot be fixed in unbiased way. In this sense, we strongly believe that any theoretical model for such complex oxide materials should be based on the results of first-principles electronic structure calculations. Otherwise it could be just an abstract mathematical construction deprived of clear physical grounds. On the other hand, it would be also incorrect to underestimate the impact of model physics on the first-principles electronic structure calculations. Certainly, one good example of such a beneficial collaboration is the problem of on-site Coulomb correlations.[2–4]

The present work clearly demonstrates that nowadays the idea of constructing the *ab initio* models for the strongly correlated systems is quite feasible: all model parameters in our work, including the intra-atomic Coulomb interactions, have been derived from the first-principles calculations using the method proposed in Ref. 34. Apart from the approximations inherent to this method, the procedure of constructing the model Hamiltonian was totally parameter free, and our analysis *did not rely on the use of any adjustable parameters*. Therefore, it is remarkable that using such a parameter-free approach we could propose a consistent explanation for a number of puzzling properties of the distorted t_{2g} perovskite oxides. The first results are really encouraging and we would like to hope that this method can be successfully applied in the future for the analysis of electronic and magnetic properties of other narrow-band materials.

It is also remarkable that the results of full-potential all-electron LDA+*U* calculations (Refs. 27 and 29) can be successfully reproduced in our model approach for the isolated t_{2g} bands. We could easily rationalize the main results of these relatively heavy calculations and elucidate the main microscopic interactions responsible for the formation of different magnetic structures in the case of $YTiO_3$, YVO_3, and $LaVO_3$. We argue that the nonsphericity of the Madelung potential should be an indispensable ingredient of both model analysis and electronic structure calculations, and the results of commonly used atomic-spheres approximation should be corrected in order to include these effects.

The crystal distortion plays an important role in the physics of t_{2g} perovskite oxides. At least for $YTiO_3$, YVO_3, and $LaVO_3$, the knowledge of the experimental lattice parameters and the atomic positions greatly helps in explaining the magnetic properties of these compounds. Of course, some questions still remain. Particularly, what is the origin of this distortion? Why is it so different for different compounds, that is finally manifested in the formation of completely different magnetic structures? Very similar arguments have been employed in order to explain the magnetic behavior of $LaMnO_3$, which is a characteristic example of the Jahn-Teller distorted e_g perovskite oxides. Particularly, it was argued that the experimental distortion not only stabilize the *A*-type AFM ground state of $LaMnO_3$,[67,72–74] but is also responsible for the opening of the band gap.[72,74] However, the direction of the Jahn-Teller distortion in $LaMnO_3$ can be naturally under-

stood in terms of anharmonicity of the electron-lattice interaction.[54,75,76] In this sense, $LaMnO_3$ is an easy example. Then, is it possible to rationalize the behavior of t_{2g} perovskite oxides in a similar way and come up with some suitable lattice model, which would explain not only the direction of the lattice distortion in each particular compound, but also the difference between these compounds?

Finally, we emphasize the importance of correlation effects in the t_{2g} band of distorted perovskite oxides. Although the mean-field Hartree-Fock approach provides a satisfactory description for the magnetic properties of $YTiO_3$, YVO_3, and $LaVO_3$, the inclusion of the correlation effects systematically improves the agreement with the experimental data for all three compounds. Definitely, $LaTiO_3$ is an exceptional example for which we could not obtain the correct *G*-type AFM ground state neither at the level of Hartree-Fock approximation nor after including some correlation effects, though in a very approximate form. However, we expect that the situation may change by systematically improving the level of approximations for treating the correlation effects. The approximations considered in the present work were simply not enough in the case of $LaTiO_3$.

ACKNOWLEDGMENTS

The author is grateful to Masatoshi Imada for valuable discussions. This work has been partially supported by Grants-in-Aid for Scientific Research in Priority Area "Anomalous Quantum Materials" from the Ministry of Education, Culture, Sports, Science and Technology of Japan.

*Electronic address: solovyev.igor@nims.go.jp

[1] M. Imada, A. Fujimori, and Y. Tokura, Rev. Mod. Phys. **70**, 1039 (1998); Y. Tokura and N. Nagaosa, Science **288**, 462 (2000).
[2] V. I. Anisimov, J. Zaanen, and O. K. Andersen, Phys. Rev. B **44**, 943 (1991).
[3] I. V. Solovyev, P. H. Dederichs, and V. I. Anisimov, Phys. Rev. B **50**, 16861 (1994).
[4] V. I. Anisimov, A. I. Poteryaev, M. A. Korotin, A. O. Anokhin, and G. Kotliar, J. Phys.: Condens. Matter **9**, 7359 (1997); S. Y. Savrasov, G. Kotliar, and E. Abrahams, Nature (London) **410**, 793 (2001); K. Held, G. Keller, V. Eyert, D. Vollhardt, and V. I. Anisimov, Phys. Rev. Lett. **86**, 5345 (2001); A. I. Lichtenstein and M. I. Katsnelson, Phys. Rev. B **57**, 6884 (1998).
[5] Y. Imai, I. Solovyev, and M. Imada, Phys. Rev. Lett. **95**, 176405 (2005).
[6] D. A. Maclean, H.-N. Ng, and J. E. Greedan, J. Solid State Chem. **30**, 35 (1979).
[7] M. Itoh, M. Tsuchiya, H. Tanaka, and K. Motoya, J. Phys. Soc. Jpn. **68**, 2783 (1999).
[8] J. Akimitsu, H. Ichikawa, N. Eguchi, T. Miyano, M. Nishi, and K. Kakurai, J. Phys. Soc. Jpn. **70**, 3475 (2001).
[9] C. Ulrich, G. Khaliullin, S. Okamoto, M. Reehuis, A. Ivanov, H. He, Y. Taguchi, Y. Tokura, and B. Keimer, Phys. Rev. Lett. **89**, 167202 (2002).
[10] F. Iga, M. Tsubota, M. Sawada, H. B. Huang, S. Kura, M. Takemura, K. Yaji, M. Nagira, A. Kimura, T. Jo, T. Takabatake, H. Namatame, and M. Taniguchi, Phys. Rev. Lett. **93**, 257207 (2004).
[11] B. Keimer, D. Casa, A. Ivanov, J. W. Lynn, M. v. Zimmermann, J. P. Hill, D. Gibbs, Y. Taguchi, and Y. Tokura, Phys. Rev. Lett. **85**, 3946 (2000).
[12] M. Cwik, T. Lorenz, J. Baier, R. Müller, G. André, F. Bourée, F. Lichtenberg, A. Freimuth, R. Schmitz, E. Müller-Hartmann, and M. Braden, Phys. Rev. B **68**, 060401(R) (2003).
[13] Y. Ren, T. T. M. Palstra, D. I. Khomskii, E. Pellegrin, A. A. Nugroho, A. A. Menovsky, and G. A. Sawatzky, Nature (London) **396**, 441 (1998).
[14] G. R. Blake, T. T. M. Palstra, Y. Ren, A. A. Nugroho, and A. A. Menovsky, Phys. Rev. B **65**, 174112 (2002).
[15] A. A. Tsvetkov, F. P. Mena, P. H. M. van Loosdrecht, D. van der Marel, Y. Ren, A. A. Nugroho, A. A. Menovsky, I. S. Elfimov, and G. A. Sawatzky, Phys. Rev. B **69**, 075110 (2004).
[16] C. Ulrich, G. Khaliullin, J. Sirker, M. Reehuis, M. Ohl, S. Miyasaka, Y. Tokura, and B. Keimer, Phys. Rev. Lett. **91**, 257202 (2003).
[17] V. G. Zubkov, G. V. Bazuev, V. A. Perelyaev, and G. P. Shveikin, Sov. Phys. Solid State **15**, 1079 (1973).
[18] P. Bordet, C. Chaillout, M. Marezio, Q. Huang, A. Santoro, S-W. Cheong, H. Takagi, C. S. Oglesby, and B. Batlogg, J. Solid State Chem. **106**, 235 (1993).
[19] T. Mizokawa and A. Fujimori, Phys. Rev. B **54**, 5368 (1996).
[20] G. Khaliullin and S. Maekawa, Phys. Rev. Lett. **85**, 3950 (2000).
[21] P. Horsch, G. Khaliullin, and A. M. Oleś, Phys. Rev. Lett. **91**, 257203 (2003).
[22] G. Khaliullin and S. Okamoto, Phys. Rev. Lett. **89**, 167201 (2002).
[23] M. Mochizuki and M. Imada, Phys. Rev. Lett. **91**, 167203 (2003).
[24] R. Schmitz, O. Entin-Wohlman, A. Aharony, A. B. Harris, and E. Müller-Hartmann, Phys. Rev. B **71**, 144412 (2005).
[25] H. Fujitani and S. Asano, Phys. Rev. B **51**, 2098 (1995).
[26] H. Sawada, N. Hamada, K. Terakura, and T. Asada, Phys. Rev. B **53**, 12742 (1996).
[27] H. Sawada and K. Terakura, Phys. Rev. B **58**, 6831 (1998).
[28] I. V. Solovyev, Phys. Rev. B **69**, 134403 (2004).
[29] Z. Fang and N. Nagaosa, Phys. Rev. Lett. **93**, 176404 (2004).
[30] E. Pavarini, S. Biermann, A. Poteryaev, A. I. Lichtenstein, A. Georges, and O. K. Andersen, Phys. Rev. Lett. **92**, 176403 (2004).
[31] E. Pavarini, A. Yamasaki, J. Nuss, and O. K. Andersen, New J. Phys. **7**, 188 (2005).
[32] S. V. Streltsov, A. S. Mylnikova, A. O. Shorikov, Z. V. Pchelkina, D. I. Khomskii, and V. I. Anisimov, Phys. Rev. B **71**, 245114 (2005).
[33] S. Okatov, A. Poteryaev, and A. Lichtenstein, cond-mat/0412063 (unpublished).
[34] I. V. Solovyev, Phys. Rev. B **73**, 155117 (2005).
[35] There are certain experimental indications that the actual symmetry of the intermediate phase of YVO_3 can be even lower than $P2_1/a$ (Ref. 15).
[36] For example, from the viewpoint of superexchange interactions, it is more natural to define the "orthogonal" orbitals as the ones

which are decoupled via matrix elements of transfer integrals between neighboring transition-metal sites: $\langle \phi_{\mathbf{R}} | \hat{h}_{\mathbf{RR}'} | \phi_{\mathbf{R}'} \rangle = 0$, which is not always the same as the regular orthogonality condition (Ref. 28).

[37] O. K. Andersen, Phys. Rev. B **12**, 3060 (1975); O. Gunnarsson, O. Jepsen, and O. K. Andersen, *ibid.* **27**, 7144 (1983); H. L. Skriver, *The LMTO Method* (Springer-Verlag, Berlin, 1984); O. K. Andersen, Z. Pawlowska, and O. Jepsen, Phys. Rev. B **34**, 5253 (1986).

[38] The Wannier functions have been calculated using the method proposed in Ref. 34. In these calculations, the Wannier functions for the t_{2g} bands have been orthogonalized to the O($2p$), Ti(e_g), and Y($4d$) bands, in the case of $YTiO_3$; O($2p$), Ti(e_g), and La($5d6sp$) bands, in the case of $LaTiO_3$; O($2p$), V(e_g), and Y($4d$) bands, in the case of YVO_3; and O($2p$), V(e_g), and La($5d$) bands, in the case of $LaVO_3$. We have confirmed that such an accuracy is sufficient in order to calculate the CF splitting caused by the nonsphericity of the Madelung potential (2).

[39] N. Marzari and D. Vanderbilt, Phys. Rev. B **56**, 12847 (1997).

[40] J. Kanamori, Prog. Theor. Phys. **17**, 177 (1957).

[41] M. W. Haverkort, Z. Hu, A. Tanaka, G. Ghiringhelli, H. Roth, M. Cwik, T. Lorenz, C. Schüssler-Langeheine, S. V. Streltsov, A. S. Mylnikova, V. I. Anisimov, C. de Nadai, N. B. Brookes, H. H. Hsieh, H.-J. Lin, C. T. Chen, T. Mizokawa, Y. Taguchi, Y. Tokura, D. I. Khomskii, and L. H. Tjeng, Phys. Rev. Lett. **94**, 056401 (2005).

[42] C. J. Bradley and A. P. Cracknell, *The Mathematical Theory of Symmetry in Solids* (Clarendon, Oxford, 1972).

[43] Note that in order to improve ASA for the loosely packed atomic structures, several empty spheres have been added in the process of LMTO calculations. A typical example for $YTiO_3$ is given in Ref. 34. These spheres are negatively charged ($Z^*_{\mathbf{R}} < 0$) and some of them are located in the nearest neighborhood to the transition-metal sites. The contribution of these spheres to the Madelung potential can make some difference from the conventional form of the CF splitting expected from the point-charge model.

[44] O. Gunnarsson, O. K. Andersen, O. Jepsen, and J. Zaanen, Phys. Rev. B **39**, 1708 (1989); O. Gunnarsson, A. V. Postnikov, and O. K. Andersen, *ibid.* **40**, 10407 (1989); V. I. Anisimov and O. Gunnarsson, *ibid.* **43**, 7570 (1991); I. V. Solovyev and P. H. Dederichs, *ibid.* **49**, 6736 (1994).

[45] J. Kanamori, Prog. Theor. Phys. **30**, 275 (1963).

[46] Note that the definition of Kanamori parameters $\mathcal{U}$ and $\mathcal{J}$ is different from the parameters U and J, which are typically used in LDA+U calculations (Ref. 3). Nevertheless, there are simple relations connecting these two sets of parameters: $\mathcal{U} = U + \frac{8}{7}J$ and $\mathcal{J} \simeq 0.77J$.

[47] J. Zaanen and G. A. Sawatzky, J. Solid State Chem. **88**, 8 (1990).

[48] A. I. Liechtenstein, M. I. Katsnelson, V. P. Antropov, and V. A. Gubanov, J. Magn. Magn. Mater. **67**, 65 (1987); I. V. Solovyev, in *Recent Research Developments in Magnetism and Magnetic Materials* (Transworld Research Network, India, 2003), Vol. 1, pp. 253–294.

[49] J. Friedel and C. M. Sayers, J. Phys. (France) **38**, 697 (1977); F. Kajzar and J. Friedel, *ibid.* **39**, 397 (1978); G. Treglia, F. Ducastelle, and D. Spanjaard, *ibid.* **41**, 281 (1980).

[50] A. Georges, G. Kotliar, W. Krauth, and M. J. Rozenberg, Rev. Mod. Phys. **68**, 13 (1996).

[51] R. Shiina, T. Nishitani, and H. Shiba, J. Phys. Soc. Jpn. **66**, 3159 (1997); L. F. Feiner and A. M. Oleś, Phys. Rev. B **59**, 3295 (1999).

[52] A. M. Oleś, G. Khaliullin, P. Horsch, and L. F. Feiner, Phys. Rev. B **72**, 214431 (2005).

[53] P. W. Anderson, Phys. Rev. **115**, 2 (1959).

[54] K. I. Kugel and D. I. Khomskii, Sov. Phys. Usp. **25**, 231 (1982).

[55] Note that $2/(E_S+E_T) > 1/E_S + 1/E_T$. Therefore, according to Eq. (13), two separate excitations into the singlet (S) and triplet (T) states are more favorable energetically rather than the excitation into the HF state with an averaged energy.

[56] M. Noguchi, A. Nakazawa, S. Oka, T. Arima, Y. Wakabayashi, H. Nakao, and Y. Murakami, Phys. Rev. B **62**, R9271 (2000).

[57] Note, however, that the LDA+U calculations reported in Refs. 27 and 29 for YVO_3 may overestimate the total energy difference between different magnetic states, apparently due to the double counting of the nonsphericity effects. By default, in the full-potential implementation of the LDA+U method, the nonsphericity of the on-site Coulomb and exchange-correlation potential is taken into account twice: in the LDA part and in the correction for the on-site Coulomb interactions. Therefore, the LDA part should be additionally averaged inside some atomic sphere and we believe that it is more physical to treat this part in ASA. (Ref. 34). The error caused by the double counting is expected to be larger for vanadite (d^2) compounds, which are subjected to the Hund's rule effects arising from the nonsphericity of Coulomb interactions between two t_{2g} electrons. A more general problem is related with the technical implementations of the LDA+U method (e.g., the choice of the parameter U and the form of the basis orbitals used for the correction), which probably explain further (small) differences existing between our results and the ones reported in Refs. 27 and 29, both for YVO_3 and $YTiO_3$.

[58] $8J_{12} = E(F) - E(G) + E(A) - E(C)$ and $4J_{13} = E(F) - E(G) - E(A) + E(C)$, where E is the total energy either in the pure HF approximation or after including the correlation effects.

[59] E. L. Nagaev, *Magnetics with Complex Magnetic Interactions* (Science, Moscow, 1988).

[60] Note that our scheme of calculation of the interatomic magnetic interactions is based on the infinitesimal rotations of the spin magnetic moments, which implies that the spins are classical. Therefore, the total energy of the Heisenberg model has the form (9), where $J_{\mathbf{RR}'}$ are related with the regular Heisenberg parameters $\tilde{J}_{\mathbf{RR}'}$ as $J_{\mathbf{RR}'} = S^2 \tilde{J}_{\mathbf{RR}'}$. Therefore, to be consistent with our definition of the exchange parameters, we use the classical expression also for the transition temperature and replace $S(S+1)$ by S^2. In order to use the quantum-mechanical definition for the transition temperature, it is necessary to use the same level of approximations also in the process of mapping of the total energy change onto the Heisenberg model, which is a more complex problem, because in the quantum case, the total energy remains proportional to S^2 only for the ferromagnetically coupled spins. The antiferromagnetic arrangement yields an additional prefactor α, which is specific to the geometry of the system and bounded by the following conditions: $(1+1/S) \leq \alpha \leq 1$. The latter are far from restrictive when the spin is small. Therefore, the quantum effects, which are especially important for the spin-1/2, will modify not only the expression for the transition temperature, but also the definition of the parameters of Heisenberg model.

[61] N. D. Mermin and H. Wagner, Phys. Rev. Lett. **17**, 1133 (1966); **17**, 1307(E) (1966).

[62] S. Miyasaka, Y. Okimoto, M. Iwama, and Y. Tokura, Phys. Rev. B **68**, 100406(R) (2003).

[63] We have also tried to improve the second order approximation for the correlation energy, but again using results of HF calculations as the starting point. First, we have tried to include the higher-order effects of the Coulomb correlations using Kanamori's *t*-matrix approach (Ref. 45), supplemented with the single-site approximation for the correlation energy. Second, we have tried to go beyond the single-site approximation and considered the intersite contributions to the correlation energy in the frameworks of the second order perturbation theory (Sec. IV B). Unfortunately, all these corrections do not change the overall picture for $LaTiO_3$, and the *G*-type AFM state remains unstable relative to the *A* state. Details will be presented elsewhere.

[64] M. Imada and T. Kashima, J. Phys. Soc. Jpn. **69**, 2723 (2000); T. Kashima and M. Imada, *ibid.* **70**, 2287 (2001); T. Mizusaki and M. Imada, Phys. Rev. B **69**, 125110 (2004).

[65] D. Treves, Phys. Rev. **125**, 1843 (1962); A. S. Moskvin and E. V. Sinitsyn, Sov. Phys. Solid State **14**, 2198 (1973); T. Yamaguchi, J. Phys. Chem. Solids **35**, 479 (1974); I. V. Solovyev, N. Hamada, and K. Terakura, Physica B **237-238**, 44 (1997).

[66] I. Dzyaloshinsky, J. Phys. Chem. Solids **4**, 241 (1958); T. Moriya, Phys. Rev. **120**, 91 (1960).

[67] I. Solovyev, N. Hamada, and K. Terakura, Phys. Rev. Lett. **76**, 4825 (1996).

[68] Note that since the angle between vectors **a** and **b** in the monoclinic structure is close to 90°, it is convenient to discuss the noncollinear magnetic structures in the orthorhombic coordinate frame, even for monoclinic symmetries.

[69] I. V. Solovyev, Phys. Rev. B **55**, 8060 (1997).

[70] M. Reehuis, C. Ulrich, P. Pattison, B. Ouladdiaf, M. C. Rheinstädter, M. Ohl, L. P. Regnault, M. Miyasaka, Y. Tokura, and B. Keimer, Phys. Rev. B **73**, 094440 (2006).

[71] T. Arima, Y. Tokura, and J. B. Torrance, Phys. Rev. B **48**, 17006 (1993); Y. Okimoto, T. Katsufuji, Y. Okada, T. Arima, and Y. Tokura, *ibid.* **51**, 9581 (1995); S. Miyasaka, Y. Okimoto, and Y. Tokura, J. Phys. Soc. Jpn. **71**, 2086 (2002).

[72] N. Hamada, H. Sawada, and K. Terakura, in *Spectroscopy of Mott Insulators and Correlated Metals*, edited by A. Fujimori and Y. Tokura (Springer, Berlin, 1995); W. E. Pickett and D. J. Singh, Phys. Rev. B **53**, 1146 (1996); I. V. Solovyev and K. Terakura, in *Electronic Structure and Magnetism of Complex Materials*, edited by D. J. Singh and D. A. Papaconstantopoulos (Springer, Berlin, 2003).

[73] R. Maezono, S. Ishihara, and N. Nagaosa, Phys. Rev. B **58**, 11583 (1998).

[74] L. P. Gor'kov and V. Z. Kresin, JETP Lett. **67**, 985 (1998).

[75] J. Kanamori, J. Appl. Phys. **31**, 14S (1960).

[76] A. J. Millis, Phys. Rev. B **53**, 8434 (1996).